Naval Research Laboratory
Washington, DC 20375-5320

NRL/MR/5670--99-8390

Strain Monitoring During Construction of a Steel Box-Girder Bridge with Arrays of Fiber Bragg Grating Sensors

SANDEEP T. VOHRA
GREGG A. JOHNSON
MICHAEL D. TODD

Optical Techniques Branch
Optical Sciences Division

BRUCE DANVER
BRYAN ALTHOUSE

SFA Inc.
Largo, MD

July 30, 1999

REPORT DOCUMENTATION PAGE

Form Approved
OMB No. 0704-0188

1. AGENCY USE ONLY *(Leave Blank)*	2. REPORT DATE	3. REPORT TYPE AND DATES COVERED
	July 30, 1999	

4. TITLE AND SUBTITLE

Strain Monitoring During Construction of a Steel Box-Girder Bridge with Arrays of Fiber Bragg Grating Sensors

5. FUNDING NUMBERS

6. AUTHOR(S)

S.T. Vohra, G.A. Johnson, B. Danver,* B. Althouse,* and M.D. Todd

7. PERFORMING ORGANIZATION NAME(S) AND ADDRESS(ES)

Naval Research Laboratory
Washington, DC 20375-5320

8. PERFORMING ORGANIZATION REPORT NUMBER

NRL/MR/5670--99-8390

9. SPONSORING/MONITORING AGENCY NAME(S) AND ADDRESS(ES)

DOT

10. SPONSORING/MONITORING AGENCY REPORT NUMBER

11. SUPPLEMENTARY NOTES

*SFA Inc.
1401 McCormick Drive
Largo, MD 20770

12a. DISTRIBUTION/AVAILABILITY STATEMENT

Approved for public release; distribution unlimited.

12b. DISTRIBUTION CODE

A

13. ABSTRACT *(Maximum 200 words)*

Field performance of arrays of wavelength division multiplexed (WDM) fiber Bragg grating strain sensors is presented. Data from two field tests, carried out in February 1998 and October 1998 on an in-construction box-girder bridge, are presented and compared to data obtained from arrays of conventional sensors, where possible. The results in this report represent one of the first extensive tests of WDM Bragg grating sensor arrays on real world infrastructure. The results show that most of the well known advantages of fiber optic sensors, for example smaller array size, electromagnetic immunity, versatile data sets, easy installation, built-in telemetry and high sensitivity can be realized in real world environments.

14. SUBJECT TERMS

Fiber optic sensors

15. NUMBER OF PAGES

51

16. PRICE CODE

17. SECURITY CLASSIFICATION OF REPORT	18. SECURITY CLASSIFICATION OF THIS PAGE	19. SECURITY CLASSIFICATION OF ABSTRACT	20. LIMITATION OF ABSTRACT
UNCLASSIFIED	UNCLASSIFIED	UNCLASSIFIED	UL

NSN 7540-01-280-5500

Standard Form 298 (Rev. 2-89)
Prescribed by ANSI Std 239-18
298-102

TABLE OF CONTENTS

Strain Monitoring During Construction of a Steel Box-Girder Bridge with Arrays of Fiber Bragg Grating Sensors

Sandeep T. Vohra, Gregg A. Johnson, Michael D. Todd, Bruce Danver and Bryan Althouse

Fiber Optic Smart Structures Section, Code 5673
Naval Research Laboratory
Washington, DC 20375

1. Introduction:

The utility of fiber Bragg gratings (FBGs) for distributed strain monitoring in structures has been demonstrated in numerous laboratory experiments [1] and in limited cases on real world structures [2]. The advantages which FBGs have over their conventional strain sensing counterparts (e.g. resistive strain gauges – RSGs) include immunity from electromagnetic interference, potential for very high sensor count, small size, simple installation and built-in telemetry. These advantages have spurned wide spread research activity in the area of Bragg grating sensor technology especially for structural monitoring. This report details the performance of an FBG strain monitoring system used to measure quasi-static strain in a steel box-girder bridge - Viaduc Des Vaux - under construction near Lausanne, Switzerland. Naval Research Laboratory (NRL) has been tasked, under an inter-agency agreement with the Federal Highway Adminstration (FHWA), to install an array of FBG strain sensors on a box-girder bridge and monitor the strain response at various locations during critical construction stages of the bridge. This was motivated by the following facts about the bridge location and construction method:

- The construction of the bridge involves using a steel box-girder, which is incrementally 'launched' in order to advance it from one pylon (or pier) to the next, especially near the deepest parts in the valley.
- The box-girder is one of the largest superstructures to be launched over a record span length of over 130 meters and a deck height of over 100 meters.
- During launching the reactions (forces) are expected to be quite large, particularly when the cantilever reaches its maximum value of 130 meters. Measuring strains at various locations during this phase of construction was important from the perspective of the designer as well as construction safety.
- Measurements during various construction phases provides a unique opportunity to demonstrate FBG strain sensing system in real world environment and also allows comparison between measured FBG sensor data and data from conventional strain gauges, located nearby on the box-girder structure.

Manuscript approved June 21, 1999.

This report provides details regarding FBG array integration, summarizes the characteristics of the FBG strain sensing instrumentation system, provides information on the array installation process, describes data from strain sensor system obtained during various construction phases, analyzes strain data including comparison between FBG and conventional strain gauge data, and makes recommendations for future FBG strain sensor systems for civil infrastructures.

2. Description of the Bridge:

Economy, simplicity, site integration and the advantage of low maintenance are the main reasons for the design form of the two 1 km long Des Vaux viaducts in Switzerland. The structures are designed as steel box girder superstructures constructed of weathering steel, to be incrementally launched. With two main spans covering 130 meters on each viaduct, these are the longest spans of their kind ever to be launched. The construction method itself is fairly common and the deck height-of–up to 100 meters – means that launching is the easiest method of building this bridge. Cranes were used on some of the sections nearer to land; one viaduct has 13 piers, the other has 14. The bridge will carry the A1 motorway between Lausanne and Bern across the steeply sided Vaux valley just south-east of Lake Neuchatel. The bridge is expected to be open to traffic in 2001. Figure 1 provides a general indication of the terrain, deck height and span length of the box girder bridge.

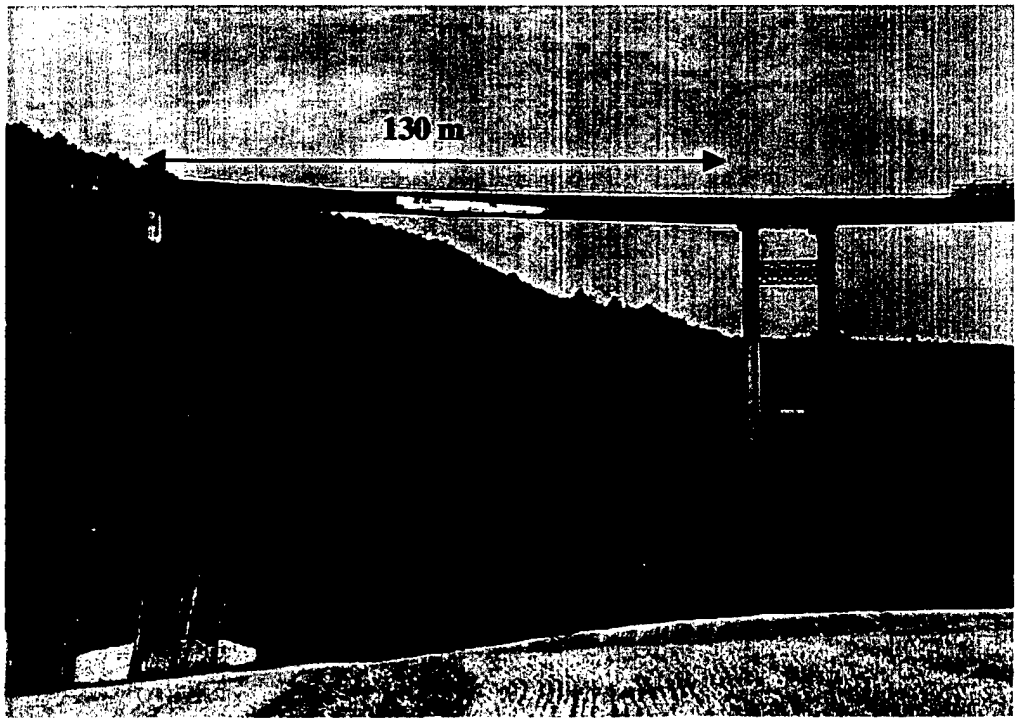

Figure 1 Picture showing the terrain, span length and deck height of Viaduct Des Vaux.

The superstructure is a 13.5 meters wide composite girder. The main spans have a variable depth steel box girder section (6 meters over the supports between the two main spans and 3.9 meters at the end of these spans) with a constant width of 6 meters. The smaller side spans have a section with two constant depth composite beams (3 meters for the 62 meter spans and 2.7 meters for the 56 meter spans). The concrete slab has a mean depth of 290 mm and it is pre-stressed both longitudinally and transversally; the pre-stressing is applied prior to the slab and the steel girders being connected together. Weathering steel is used to form the beams and box girders, which are transported to the site in half box girder pieces roughly 20 meters long and 58 ton weight, welded together on site, and then launched using a 35 meter long launching nose. Figure 2 shows a photo and a cross section of the steel box girder.

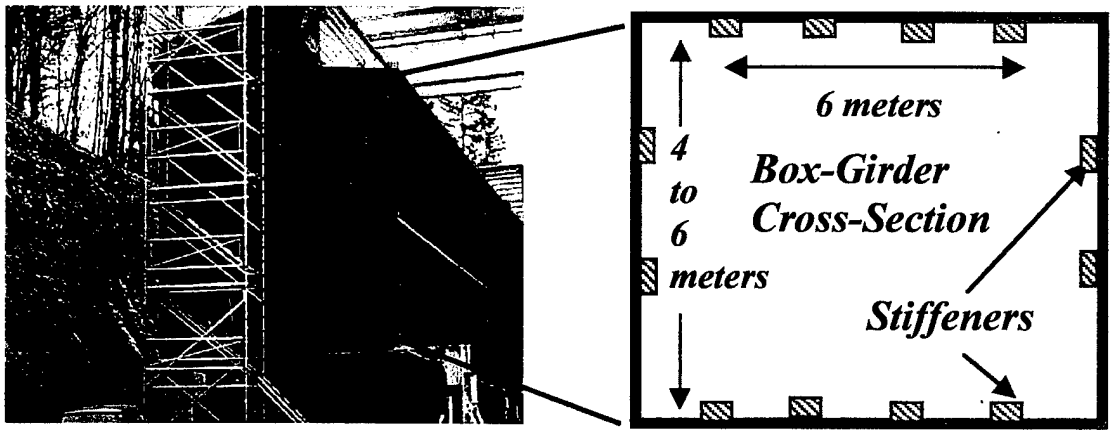

Figure 2 Photo and a sketch of the cross-section of the steel box girder. The width of the box-girder was constant at 6 meters while the height varies between 4 meters and 6 meters. The number and the position of stiffeners varied depending of the position of the box-girder with respect to the piers.

3. Description of the Box-Girder Launching Process:

As mentioned above, half box-girder pieces roughly 20 meters in length are transported to the bridge site where they are welded together. The 20 meter long box-girders are then welded length wise, while being supported on piers, near the edge of the valley. After the smaller sections are welded together to form a sufficiently long section of the box-girder, the structure is launched or 'pushed' from one pier to the next using a 35 meter long launching nose (Figure 3). The construction involved more than 14 stages of launching, with three major stages related to the 130 meter cantilevers. The big cantilever launches may be the most impressive, but all of the launches are risky and each one has to be monitored. It is not possible to monitor all 14 stages of the launching process (due to travel cost between NRL and bridge site), so this report will present data from two box-girder launches, one of which involved the 130 meter cantilever launch.

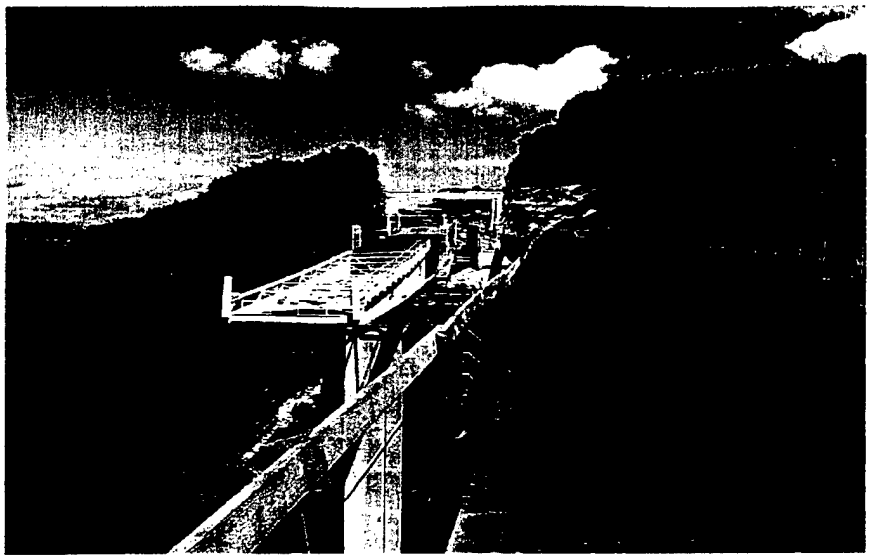

Figure 3. A picture depicting the front end of the box-girder used during launching . The launch nose is used to lift the free-end of the box-girder on to the pier. It is removed after the launch is completed.

The box-girder launching is done with a hydraulic jack located and attached to a pier near the edge of the valley. There are, in fact, two jacks one for 'pushing' the box-girder out towards the far pier while a second jack is utilized to control the rate at which the box-girder travels towards the far pier. The entire box-girder launching process is performed very carefully and no effort is spared in seeing that all safety standards are met. However, the size of the spans, the curved geometry and variable depth along with vertical reaction forces on the web during the launching process make it particularly important to monitor strains in the structure during the launching. Motivations and the types of measurements of interest are described next.

4. Motivations for distributed strain monitoring on infrastructures:

Strain monitoring at various locations on the steel box-girder structure during the launching is of interest for numerous reasons.

- Strain measurements at critical locations on the box-girder can allow for design verification and determination of structural buckling and over-loading during the launching process.
- Recording the strain history at various locations during the launch can aid in assessing structural integrity, maintenance scheduling and damage detection in the box-girder.
- For the box-girder a critical issue involves patch loading during the launching. Patch loading is the introduction of reaction loads into the web of a beam or a box-girder at a place where no vertical stiffener is provided. When the bridge is in its final position, heavy vertical stiffeners are provided over the supports and piers, allowing reactions (e.g. from traffic) to pass from the web to the supports and the piers without local buckling of

the thin webs. However, while the bridge is being launched, for the majority of time, there is no vertical stiffener over the support. Considering that the box-girder sections can undergo large reactions during launching, distinct possibility of local buckling in the bottom part of the web exits. This can damage the structure or may even cause it to collapse. Large reactions can easily occur when the cantilever reaches its maximum value of 130 meters.

• The launching operation is particularly risky for this bridge since the structure is statically non-determinate and has a large torsional stiffness. Consequently, slight modifications in the vertical positions of the sliding supports can provoke large, undesirable variations in the reactions. The curved bridge span and the variable depth are other difficulties for the launching process.

• The resistance of the webs of a box girder to transverse forces is not very well known. Most of the research carried out on patch loading has been on universal beam girders and the positive influence of longitudinal stiffeners in the bottom part of the web close to the support is not very well known. The negative effect of the initial deformations of the web due to imperfections or welding is also not very well known.

• Other very useful reasons for making distributed strain measurements on infrastructures and their payoffs are provided in reference 3.

• From an instrumentation perspective, this field test provides an excellent opportunity to try the FBG instrumentation system (grating arrays plus the wavelength shift detection scheme) in real world environment.

5. Measurements of interest on the Swiss box-girder bridge:

Considering the motivations outlined above, it was determined that measuring strain at locations inside the box-girder which are likely to see local reactions (forces) as well as global effects should be measured. Due to the fact this constitutes a test of advanced technology, the locations chosen were limited and the test period was limited to two times due to the finite size of the research funds available. We report on two test phases, each covering a different time of box-girder construction period. Sensors were bonded in locations where vertical reactions are likely to induce substantial strain on the flange and the web. Buckling of the web due to vertical reactions was of particular interest. Low frequency oscillations incurred at the free-end of a cantilever was also of interest. Propagation of local vertical influences was also of interest. The difference between lower flange and upper flange strain values was also important. Two arrays of sixteen FBGs each were attached to the box-girder during the February 1998 push phase of construction and a single array of twelve FBGs was attached during the October 1998 push phase of the box-girder construction. Details on sensor location and orientation will be provided in subsequent sections of this report. We start by describing the FBG strain sensing system.

6. Fiber Bragg Grating Sensor System – Integration and Characteristics:

The Bragg grating strain sensing system can be separated into two parts: (1) arrays of fiber Bragg gratings with appropriate spatial and spectral spacing and (2) the electro-optic instrumentation used to measure the wavelength shift in individual Bragg gratings. We begin by briefly describing the arrays of Bragg gratings.

Four separate arrays, each containing between eight and sixteen FBGs on a single fiber, with appropriate spatial separation, were prepared at NRL prior to installation. The Bragg gratings were 'shot' in photosensitive optical fibers at NRL using the method of optical interference from UV laser beams [5]. The grating periodicity was chosen such that the nominal Bragg resonance condition was near 1300 nano-meter wavelength. Two of the four arrays were installed on the bridge during early part of February 1998 while the other two were installed on the bridge in October 1998.

The FBG arrays were illuminated using an ELED operating near 1300 nm. Since the spectral characteristic of the ELED output has a Gaussian-like distribution, reflectivities of the FBGs were tailored such that the gratings with high reflectivity were near the wings of the ELED spectrum while FBGs with lower reflectivities were near the center of the ELED spectrum. This ensured approximately equal amounts of light being reflected from all the FBG sensors, thus minimizing variation in the SNR amongst individual FBG sensors.

Numerous methods have been developed for detecting the wavelength shift in a Bragg grating due to thermo-mechanical changes [6]. One of the more successful techniques for interrogating FBG sensors involves the use of tunable Fabry-Perot (FP) filter for tracking the FBG signal. In this approach, the light reflected back from an array of Bragg grating sensors is passed through a FP filter which passes one narrowband wavelength component, depending on the spacing between the mirrors in the device. As the filter is tuned by changing the mirror spacing electrically with piezoelectric stacks, the pass-band scans over the return signals from the gratings, and the wavelengths can be determined and recorded from the voltage applied to the filter. For the field test reported in this work, a scanning FP system similar to the one just described was used to interrogate arrays attached to the structure.

A schematic of a four channel scanning FP system used is shown in Figure 4. The optics includes two 1.3 μm broadband sources (edge-emitting LEDs (ELED)) having a ~35 nm full width at half maximum (FWHM), three 2x2 (3dB) couplers, one FP filter and one photo detector. The light from two ELEDs is directed through a pair of 2x2 couplers, then reflected from the multiple FBG sensors and returned through the third coupler. Finally the reflected light is transmitted to a scanning FFP filter and to a photo detector. The free spectral range (FSR) and the resolution bandwidth along with the spectral spacing between the FBGs determine the number of FBG sensors, which can be interrogated per one scan of the FP filter. The fiber Fabry-Perot filter used in this work had an FSR of about 45 nm, thus allowing 16 individual sensors, spaced by

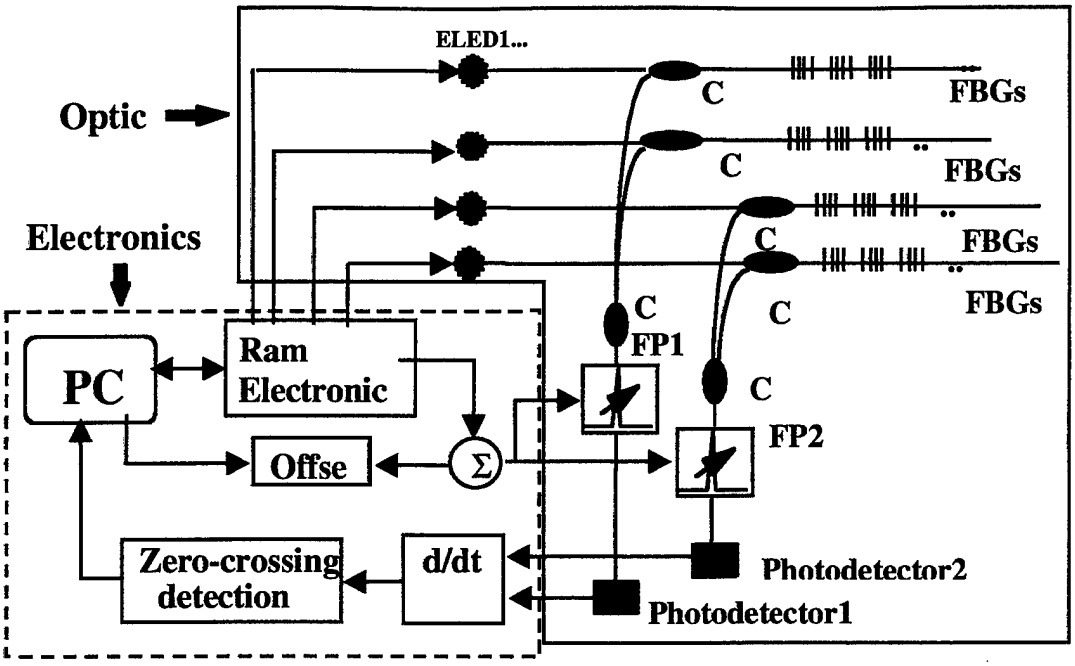

Figure 4. Schematic of a four channel scanning Fabry-Perot system used to measure the wavelength shift detection of individual gratings in the FBG arrays. C designates an optical coupler and FP designates a Fabry-Perot filter.

approximately 2.7 nm to be interrogated per filter scan. This spacing is sufficient to allow strains of about ±1300 με for each FBG to be easily monitored. As can be seen in Figure 4, two ELEDs are used to illuminate two arrays of 16 FBG sensors each. The ELEDs are synchronized with the FFP ramp signal in such a way that ELED-1 is switched on and ELED-2 is switched off during one ramp cycle of the FFP while the reverse (i.e. ELDE-1 is turned off and ELED-2 is turned on) takes place during the second ramp scanning cycle of the FFP. This source switching cycle technique controlled by the computer permits addressing only one of the two FBG arrays at any given time thus minimizng the number of expensive FFP filters in the system. The multiple Bragg spectra transmitted through the FFP filter and received by the photo detector is then electronically differentiated. This produces a series of pulses for each of the signal reflected by the FBGs with the zero-crossing of each pulse representing the peak reflected wavelength from each sensor. The zero-crossings of this signal is recorded by a computer along with the digital value (16 bits) of the ramp voltage applied to the FFP system. By referencing any shifts in the zero-crossings from each FBG to the voltage applied to the FFP filter, the strain of each sensor can be obtained.

The choice of 16 bit resolution for the FP ramp, and a FSR of 45 nm produces a minimum detectable wavelength shift of 0.7 pm, or equivalent strain resolution of less than 1 με. However, the actual minimum detectable strain is limited to about ± 2 με due

to electronic noise in the system. The FFP filter is capable of achieving scan rates of about 360 Hz and supporting 64 FBGs but in this work the system was set to operate such that the data was averaged many times and only the up-scan of the FFP ramp cycle was used. This was driven by two reasons: (1) only the up scan was used to prevent the hystersis difference of voltage-to-wavelength tuning response between the up and down scan, and (2) the FBG sensor readings were averaged a number of times (about 128) to provide better resolution (± 0.5 micro-strain). It should be pointed out that in monitoring large scale structures, static and quasi-static strains (< 10 Hz) are of prime interest and in the particular case of the structure being reported here, data was sampled at a rate of 2.8 Hz. The seemingly low data rate is also driven by the fact that there is limited memory in the computer for data storage and more importantly the events of interest are taking place on time scales which are on the order of many seconds to many minutes. For instance, the push phase of the box-girder took over 5 hours and the pull-up phase took about 2 hours. No dynamic strain effects are expected during these phases and therefore an effective sampling rate of 2.8 Hz is considered adequate.

The performance characteristics of the scanning Fabry-Perot system used to monitor the FBG wavelength shift can be summarized as follows: (i) effective scan rate = 2.8 Hz, (ii) system noise = ± 0.5 micro-strain and (iii) number of addressable FBGs = 31. System drift was measured to be under 10 micro-strain over a period of 5 hours. The performance characteristics were deemed appropriate for the field test. A picture of a typical Fabry-Perot unit used during the test is shown below.

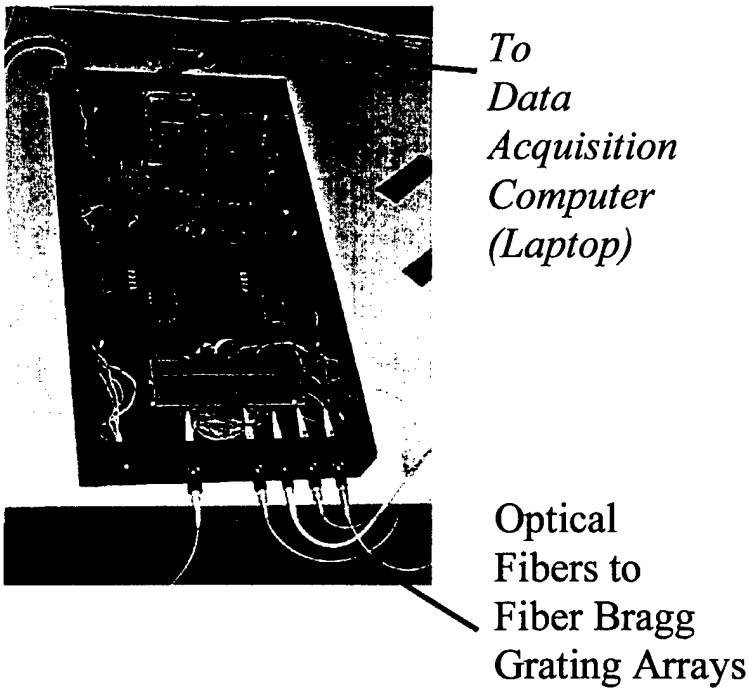

7. FBG Array Location and Installation (February 1998 Test):

The distributed strain measurements on the box-girder bridge took place during two different construction periods. The first period was in early February 1998 when one of the two 'big' push phases of construction occurred. The primary measurements of interest involved measuring strain near the free hanging end of the bridge as well as near the region in the bridge close to one of the pylons from which the cantilever started. A schematic of the box-girder prior to the 'big' push phase and the expected position of the box-girder after the push are shown in Figure 5.

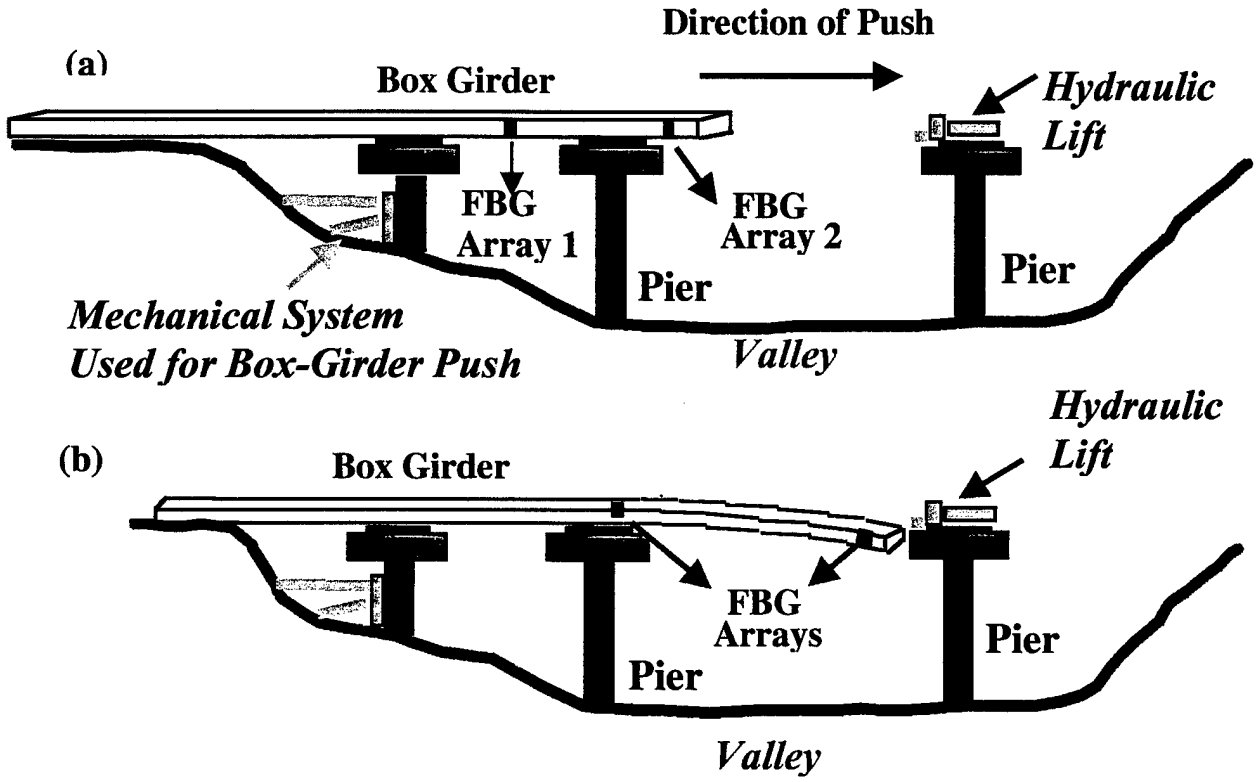

Figure 5. Schematic depicting the approximate position of the box-girder bridge (a) prior to and (b) immediately after the push. The relative positions of the FBG arrays in the structure are also shown. The grating were attached on the inside of the structure.

The Bragg gratings were attached on the inside of the 'hollow' box-girder structure at various locations as shown in Figure 6. Recall that the approximate dimensions of the box-girder tend to vary in the vertical direction (3.9 meters to about 6 meters) and remains fixed in the horizontal direction at 6 meters (see Figure 2).

In the first phase of the measurements, there was interest in not only measuring the strain at locations indicated in Figures 5 and further detailed in figure 8 but also in verifying the measurements obtained with FBG strain sensors with conventional resistive

strain gauges where possible. Therefore, an attempt was made to locate some of the FBG sensors close to conventional gauges. The research group from Ecole Polytechnique De Federeal Lausanne (EPFL), had placed approximately 75 conventional strain sensors including a substantial number of strain sensor rosettes near the locations indicated in figure 5.

Since this was the first time that Bragg grating sensors were being used to measure the strain on a box-girder bridge during the push phase it was deemed necessary to temperature compensate every Bragg grating strain response. This assumption was motivated by the fact that it takes almost an entire day for the push and pull-up phases to be completed, during which time the temperature in the valley and on the bridge can change substantially, especially on a sunny day. Therefore, out of 31 FBGs available for strain sensing, approximately half were utilized for temperature compensation. For every FBG in mechanical contact with the structure, there was a second FBG located within a few centimeters of it which was thermally attached to the structure while remaining mechanically isolated. In other words, two FBGs were used to make a measurement at every location. As will become clear in the results section, this turns out to be an unwise use of FBGs since on such a large steel structure thermal compensation of FBG response at every location is unnecessary.

7.1 Sensor Location and Orientation:

We have labeled the cantilevered region containing the FBGs as FBG array 2 and the array close to the pylon is labeled FBG array 1, as indicated in Figure 6. The location of the two arrays (Array 1 and Array 2) for the February 1998 test is shown in Figure 6. Array 1 was situated inside the box-girder at a location about 15 meters prior to pier 1. The motivation behind choosing this location was to measure the longitudinal strains in the web (side-walls) and the flange (floor, ceiling) of the box-girder due to reactions produced during the approach and the pass over the pier. There are no ceiling sensors on array 1 since it was not possible to reach the ceiling at that location with the available equipment. Array 2 is located, approximately 50 meters away from array 1, towards the free end of the box-girder (Figure 6). The motivation behind locating FBG array 2 near the cantilevered end was to be able to measure extremely low frequency oscillations of the free-end during the push phase. Additionally, it is anticipated that during the 'pull-up' phase, which involves lifting the cantilevered end on to pier 2, there should be substantial strains generated at locations of array 1 and array 2. The FBG array locations are shown in Figure 6.

All FBGs during the February 1998 test were oriented such that they measure the strain in the 'long direction' or longitudinal direction of the bridge. This was primarily driven by direction from EPFL-ICOM team on-site. Effort was made to locate FBG sensors close to conventional ones. Data from the FBG strain sensors then were measured and compared with data from conventional sensors where possible.

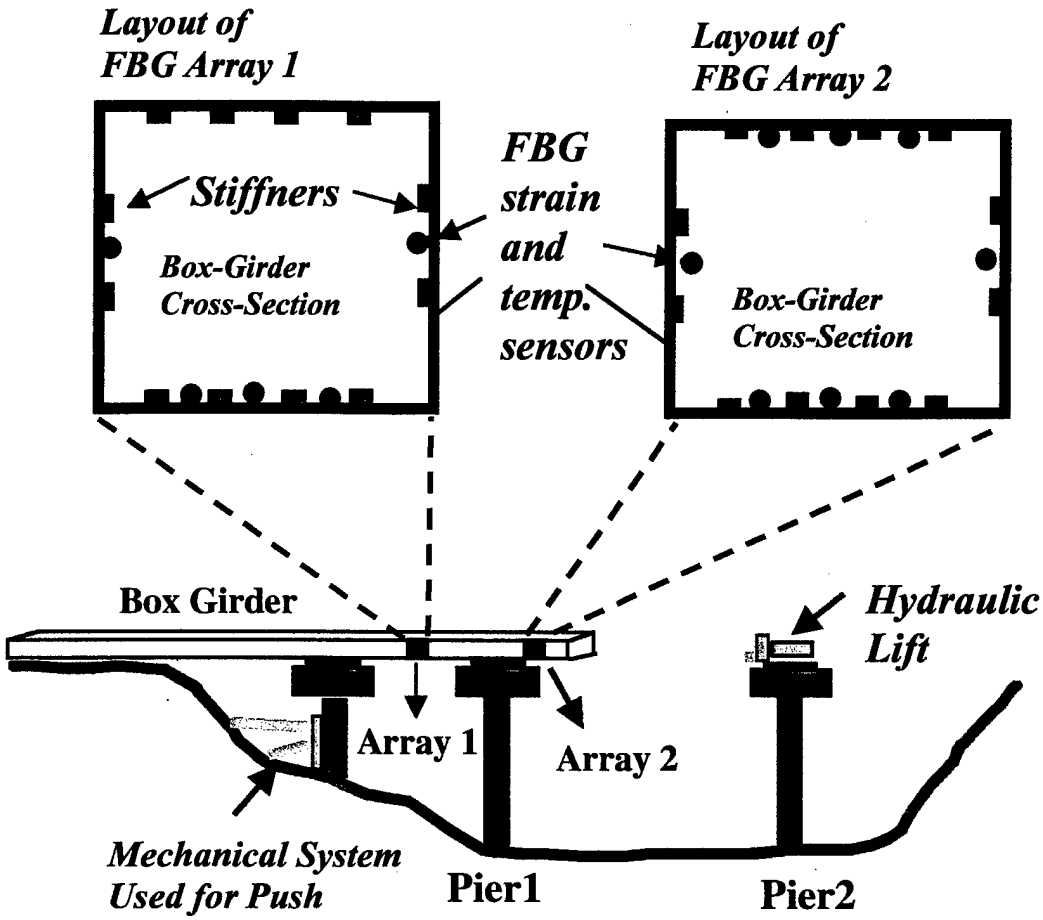

Figure 6 Locations of the two arrays in the box-girder along with the arrangement of individual FBGs at within each of the array.

7.2 FBG Sensor Attachment:

Since the inside walls of the box-girder structure were completely covered with a layer of rust and other debris, the surface was first prepared for attaching the Bragg gratings to steel. This was accomplished by first sweeping the debris from the immediate surroundings of the chosen location, followed by sanding the region (typically 25 cm x 7 cm) with an electric sander in order to remove the rust until the steel surface of the box-girder could be seen. The relatively smooth steel surface was then cleaned with a two part cleaning solution to reveal a dust and rust free steel surface. A slight pre-strain was applied to the Bragg gratings meant for measuring the structural strain were subsequently attached to the surface using an acrylate based adhesive (M-bond 2000 - a common strain gauge adhesive). The gratings were lightly coated with 'five-minute' epoxy for protection from wetness and better mechanical strength. A second grating meant for measuring the

temperature of the structure was placed very close to the first grating but not physically attached to the structure. Thermal heat sink compound was used to attach the 'thermal' grating to the structure. The expectation was that the thermal heat sink compound would keep the grating mechanically isolated from the structure while making good thermal contact. As it turned out, this approach was faulty since at low temperatures the heat-sink compound tends to become quite stiff and allows for a degree of mechanical coupling to the structure. Fortunately, thermal drifts during data collection turned out to be a non-issue since significant changes in temperature on large steel structures are not expected to occur rapidly, aided by the fact that the temperature remained constant (low) throughout the data collection period. Two arrays of sixteen FBGs each were attached to the structure in this manner.

Since the sensors were attached on the bottom flange (i.e.floor) as well as the top flange (i.e. ceiling) of the box-girder and also on the web (i.e. the side walls) it was deemed necessary to protect the floor sensors and some of the side-wall sensors from breakage due to human traffic inside the box-girder. This was accomplished by applying an inverted plastic C-channel over the Bragg grating sensors. The plastic C-channels were bonded using five minute epoxy over the sensors and taped to the structure. Figure 7 shows photographs of sensors with and without the plastic C-channels.

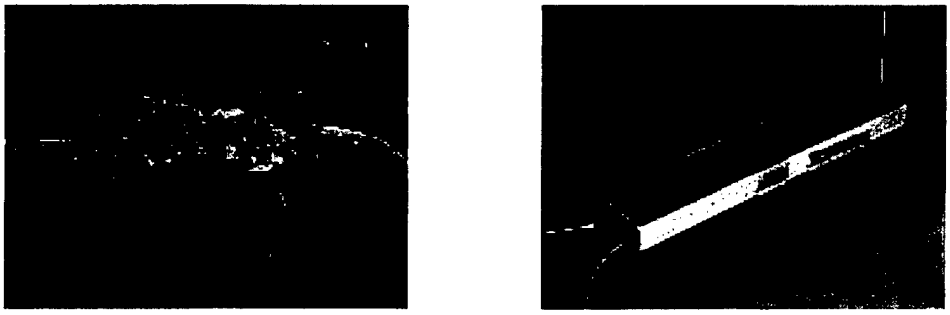

Figure 7. FBG sensor bonded on a prepared surface of the box-girder without (left) and with (right) a protective channel. Orange optical telemetry cables can also be seen.

After the attachment of the FBG arrays inside the box-girder, the telemetry cable, which was Kevlar reinforced for providing strength and protection, was routed through small openings in the structure towards the top of the box-girder and eventually to the point from where the measurements were taken. Measurements were taken from atop a pier, adjacent to pier 1 as shown in Figure 8. The adjacent pier is meant for a second box-girder to be placed after the completion of the first one. The second box-girder is meant for traffic in the opposite direction, however at the time of the February 1998 measurements contained no box-girder. Figure 8 also shows the approximate location of arrays 1 and 2, and pier 1. The far pier (pier 2), towards which the box-girder is being pushed, is hidden in the picture, however, the pier adjacent to it can be seen in the figure.

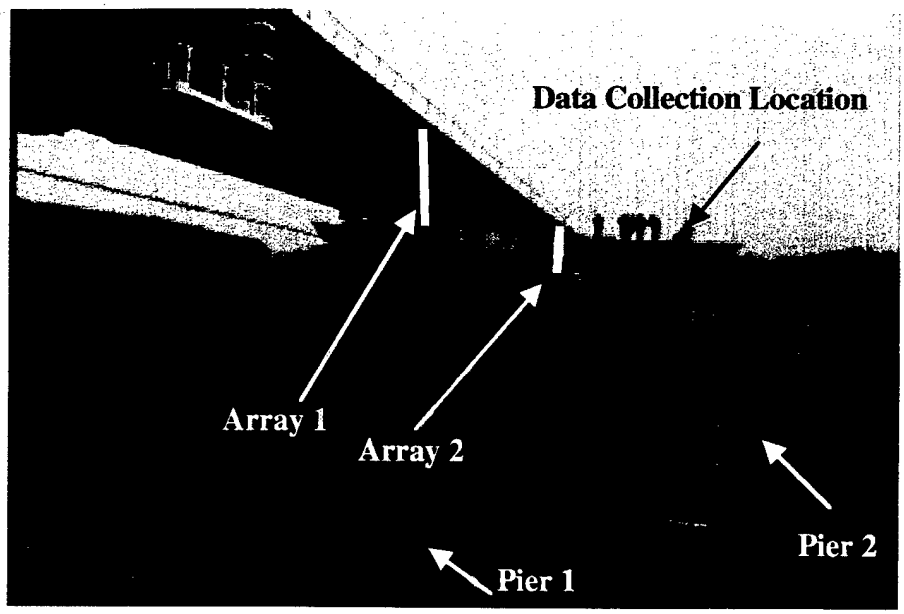

Figure 8. Photo of the box-girder prior to the push. Approximate locations of arrays 1 and 2 with respect to pier 1 and 2 are shown. The data collection location is also shown.

8. Measurements During the Push Phase of February 1998:

Before describing the measurements obtained during the push phase of February 1998, we note that the launching or the push of the box-girder is not a continuous process. Often, the push is halted for construction crew to inspect the progress as well as to determine safety. The data obtained with the FBG sensors was collected only during times when the actual launching was taking place. In other words, the data collection was stopped during times when there was no launching taking place or during other periods of inactivity (e.g. lunch break). The Fabry-Perot data collection software system was configured such that any 'new' data set always started at zero strain. For instance, if a data file was started at 9 am and stopped 30 minutes later it would start recording at zero strain and log all strain values relative to that starting strain. If this is followed by a data file starting at 11 am, it would also start at zero strain, even though from an absolute strain perspective, there might be substantial strain present at a given location. However, it is possible to piece together all the data files by providing appropriate strain offsets on each individual data file and provide the full strain history during launching.

In the subsequent discussion on strain measurements, we analyze individual data sets, for pointing out subtle features during various phases of the launch and later also provide the full strain history by piecing together the individual strain data files. Conventional gauge data was not recorded continuously but rather recorded as discrete points taken at almost random time intervals, ranging from once every few minutes to once every few hours. Unfortunately, the two clocks of the two systems were not precisely synchronized making it cumbersome, but not impossible to compare data sets.

The 130 m push occurred on February 4, 1998. Approximate position of the two FBG arrays before and at the end of the push is shown in figure 5. Preparations began very early in the morning, around 7 am. Ambient temperature was about 4-6 °F with little precipitation, although there was overnight frost and some ice on the box-girder and the piers. However, since the sensors are attached on the inside walls of the box-girder there was little chance of gratings seeing any wetness from frost. The two telemetry cables addressing the two FBG arrays, were connected to the scanning Fabry-Perot unit and the associated electro-optics allowed to 'warm-up' for at least one hour prior to the push. Electrical power was available at the pier, however the data collection computer was operated on batteries to minimize noise from its power supply. Preparations for the push were time consuming and there were many occasions in which the push was stopped for long periods of time. The data was collected only when the actual push was taking place primarily to conserve memory on the computer hard drive. We begin by showing few of the data files taken during relatively short push phases and pointing out common features. This will be followed by the full strain history obtained by piecing together the individual data files.

8.1 Data set from 9:10 am push:

The first set of data from the push phase was collected around 9:10 am. The data run is about an hour long. Figure 9 shows the measured strain data from the three sensors attached to the floor of the box girder which, are part of FBG array 1 and are located such that as the push occurs, the sensors approach pier 1. We expect compressive strain at the sensor location and figure 9 clearly depicts negative strain

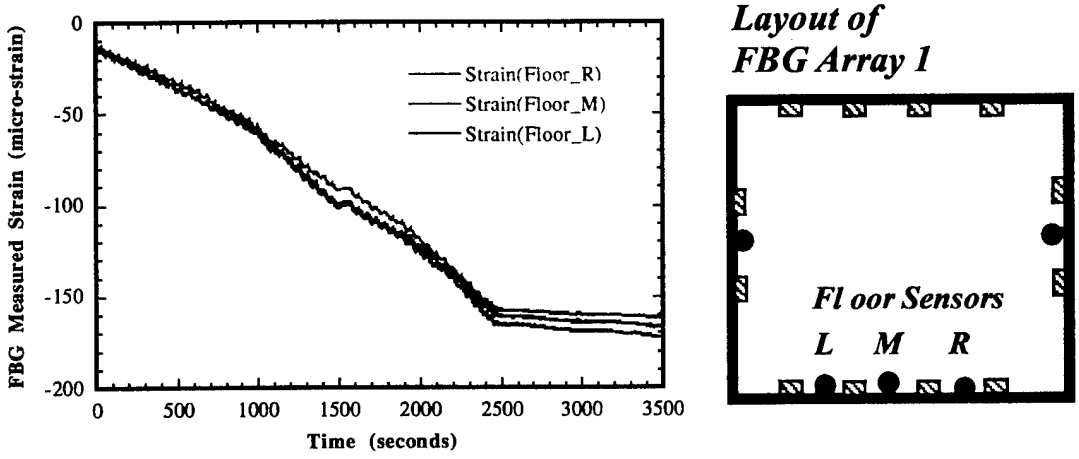

Figure 9. FBG strain data (left) from the three floor (or flange) sensors of FBG array 1 taken during the hour long push which started around 9:10 am on February 4, 1998. Corresponding sensor location on the box-girder cross-section is shown on the right. The data clearly shows compressive strain. No corresponding conventional gauge data exists for this phase since none was taken.

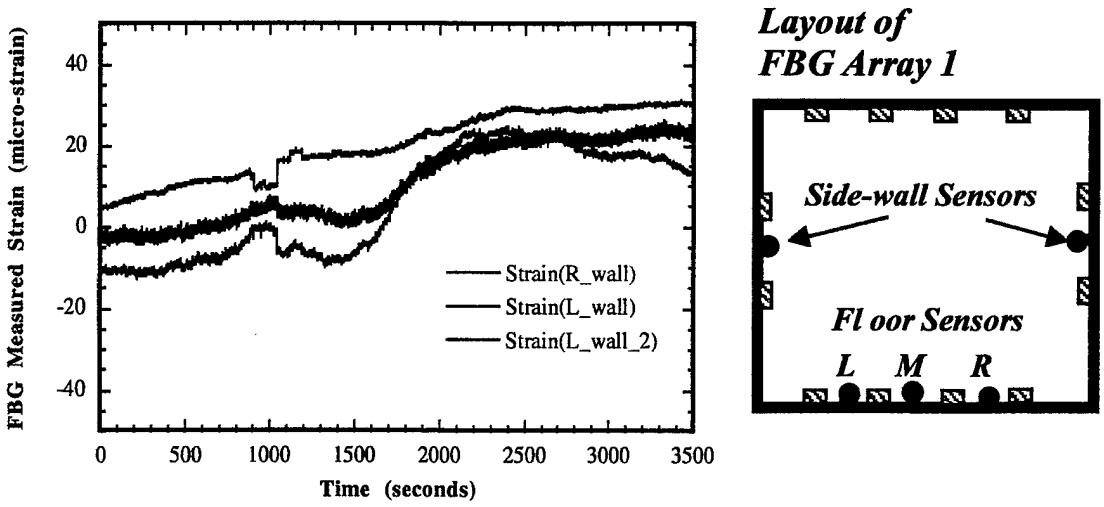

Figure 10. FBG strain data (left) from the three side-wall sensors of FBG array 1 (right) taken during the hour long push which started around 9:10 am on February 4, 1998. There are two FBG sensors on the left side-wall separated by about 3 meters longitudinally, thus there are two curves showing data from left wall sensors.

Data corresponding to FBG sensors of array 1 located on the web (i.e. side walls) are shown in figure 10. The data from the FBG sensors of array 1 located on the side-walls show significantly lower strain levels then the sensors located on the floor (Figure 9). This is attributed to the fact that the sensors on the side-walls were located close to the neutral axis of the box-girder where longitudinal strain is expected to be minimal.

Data from FBG array 2 located about 50 meters towards the front of the box-girder (see Figure 6 for sensor location details) are shown in Figure 11 and 12. The data is from the region of the box-girder located away from pier 1 and in essence corresponds to the free end of the box-girder. Therefore that region of the structure does not experience the same kind of boundary conditions as the region where FBG array 1 is located. This results in little strain developing on the flanges (both the floor and the ceiling) during the push phase as is evidenced from the data of Figure 11. The strain data from the two flange sensors (i.e. ceiling and the floor sensors) have opposite signs which indicates that the top flange experiences compression while the bottom flange experiences tension, which is consistent with the geometry of the box-girder. The data of both Figure 11 and 12 shows an initial offset in the data (at time = 0 seconds). This is due to the fact that the electro-optic system was not normalized to zero strain just prior to data collection. In other words, the strain offsets indicate actual strains at the sensor location at the initiation of data collection period.

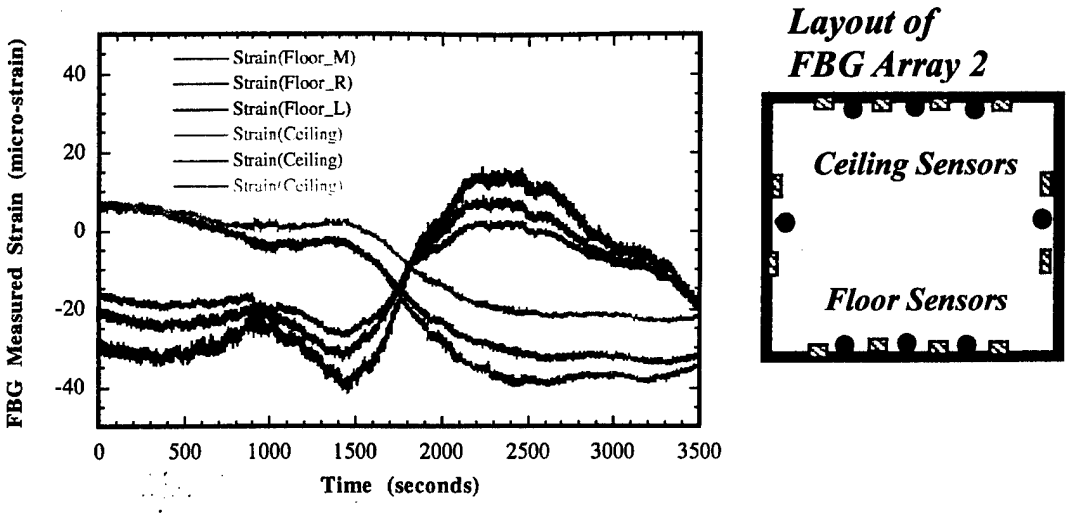

Figure 11. Data (left) from the three floor and three ceiling sensors of FBG array 2 (right). Data taken around 9:10 am on February 4, 1998.

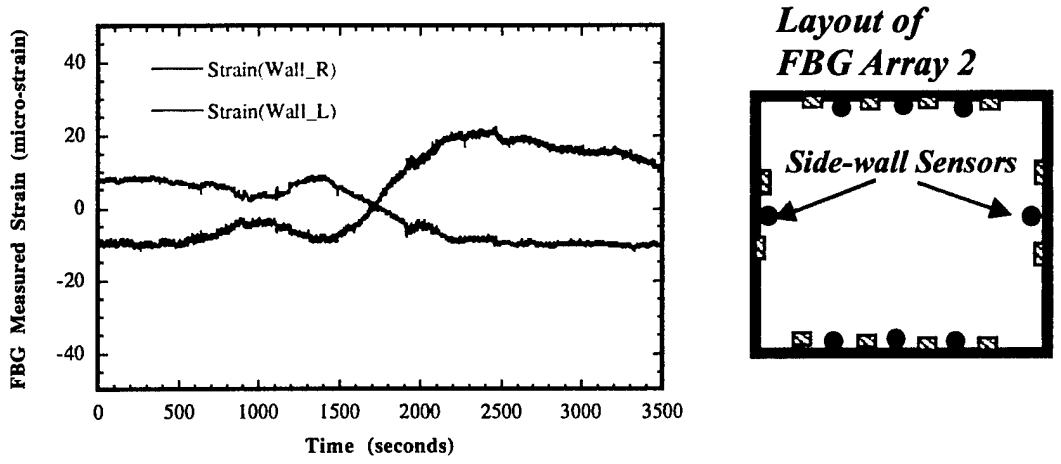

Figure 12 . Data (left) from the side-wall sensors of FBG array 2 (right). Data taken at about 9:10 am on February 4, 1998.

The data of figure 12 shows that the side-wall sensors switch signs as the push progresses. This is due to the fact that the sensors were mounted in a complimentary manner. It is likely that the sensor on the right wall was just above the neutral axis of the structure while the FBG sensor was on just below the neutral axis of the structure. This

could result in strains of different signs on the two sensors on opposite wall. It has not been possible to pinpoint the neutral axis of the structure but the data of figures 10 and 11 clearly indicates that there is little measured strain in the longitudinal direction on the side walls (i.e. webs).

The 9:10 am push was stopped by the construction crew after approximately an hour. Inspection ensued and the next phase commenced at about 11 am.

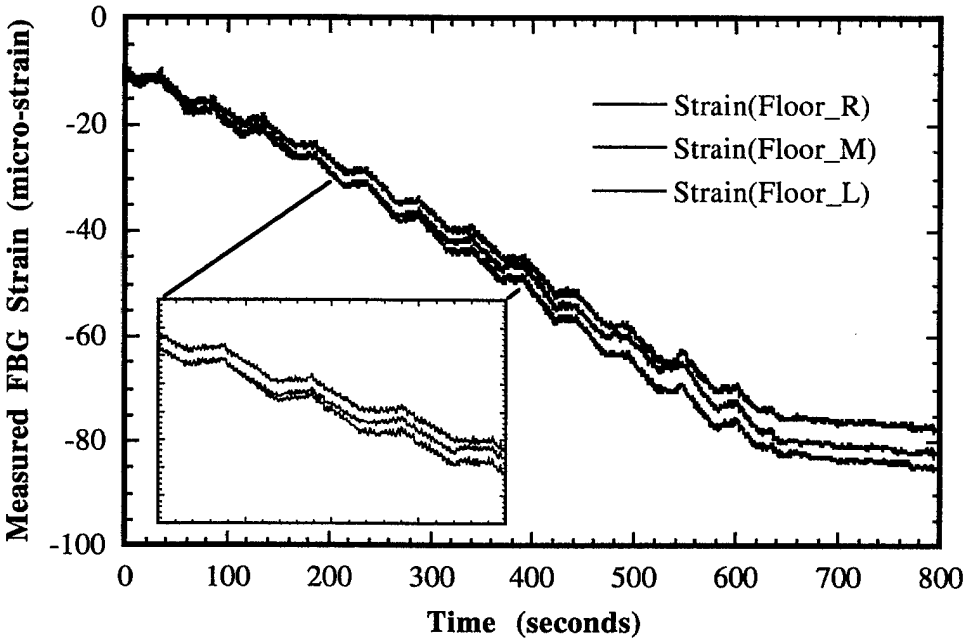

Figure 13. Data depicting strain experienced by the floor sensors of FBG array 1 during a thirteen minute push which occurred around 11:00 am. Inset shows data between 200 and 400 seconds of the entire data set.

8.2 Data set from 11 am push:

Figure 13 shows data from three floor sensors of FBG array 1, as measured during the push which started around 11 am. The data shows further compression of the flange, which is expected since the structure is approaching the pier. As previously indicated, the data set starts at about zero strain value since it constitutes a new data run. Certain interesting details that were recorded during the push will be pointed out in this section of the report. The data clearly shows a step-like push motion experienced by the box-girder. Inset of figure 13 further shows the step-like, stop and go motion with which the box-girder is being pushed by the hydraulic jack. As is the norm during the push, there is a tendency to stop to inspect various systems involved, which is clearly evident after about

625 seconds into the data. The operators have clearly stopped pushing the box-girder for inspection. Such continuous data gathering was not done with the conventional strain gauges thus making it difficult to compare such details with the resistive strain gauge data set. In fact, the EPFL-ICOM conventional gauge system was not utilized at all during these small pushes.

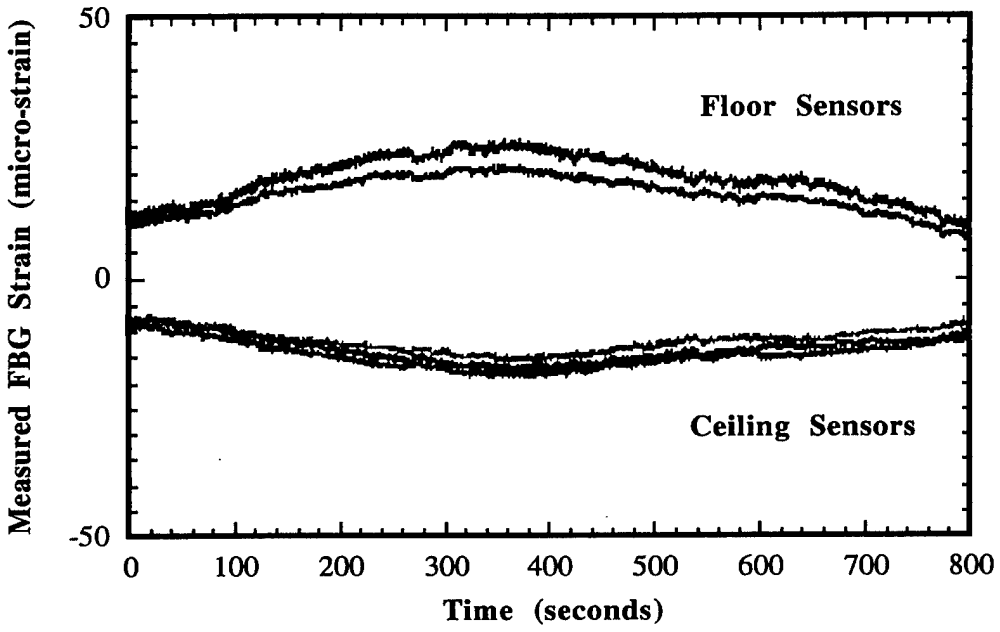

Figure 14. Data depicting strain experienced by the flange (i.e. floor and ceiling) sensors of the FBG array 2 during a thirteen minute push which occurred around 11:00 am.

Figure 14 shows the FBG strain data from the floor and ceiling sensors of FBG array 2, which is located near the cantilevered end of the box-girder. The floor sensors experience strains of approximately equal magnitude but opposite sign to that of ceiling sensors. This is expected since the ceiling and the floor sensors are located on opposite extremes of the neutral axis of the structure such that the ceiling experiences compression while the floor experiences tension. Additionally, it is pointed out that the overall magnitude of the sensors located in the region labeled FBG array 2 tend to experience lower magnitude strain than those located in the region labeled FBG array 1, as can be seen from figure14. This is consistent with the fact that the sensors of array 1 are approaching pier 1 and therefore tend to experience increased vertical reactions while sensors of FBG array 2 are close to the cantilevered end which experiences greater displacement but not necessarily large strain. The situation is analogous to a simple cantilever beam that experiences greater strain in the clamped region than near the 'free-end'.

Next we describe data from the push phase which started at about 1:25 pm on February 4, 1999 and resulted in box-girder displacement of over 20 meters thus inducing substantial strain at the location of FBG array 1. Data from FBG array 1 will be compared with data from conventional resistive strain gauges located close to the FBG array 1. A simple mathematical model, qualitatively describing the results will also be presented. Data from FBG array 1 will be emphasized since it is that array which experiences the most interesting strain fields during this part of the push phase. Additionally, conventional gauge data exists only for sensor suite located close to array 1.

8.3 Data from the 1:25 pm push phase:

Figure 15 shows data from the three floor (or the bottom flange) strain sensors of FBG array 1 as the box-girder underwent a push of about 15 meters. In other words, the location of the array prior to this particular push was slightly less than 15 meters away from pier 1. At the end of this particular push phase, the location corresponding to FBG array 1 was a few meters beyond pier 1.

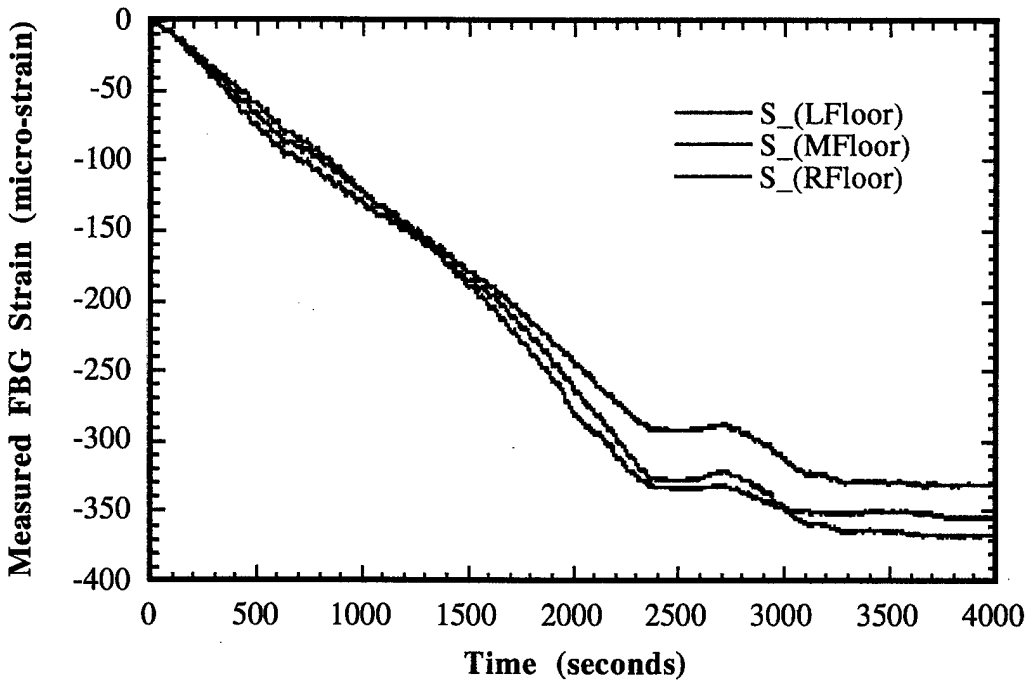

Figure 15. Strain data from the three flange (i.e.floor) sensors of FBG array 1 obtained during the push which started at about 1:25 pm on February 4, 1998.

The data shows that the three floor sensors undergo negative strain as the push occurs, eventually showing little or no strain change after about 3000 seconds in to the push. This can be qualitatively understood as follows. The Bragg gratings located in FBG array 1 tend to see compressive strains as the box-girder approaches the pier. This is evidenced by the negative strains observed in the FBG response for about 3000 seconds. The strain response shows little change in magnitude after 3000 seconds which can be attributed to the fact that at this point the array is very close to or directly above the pier, in which case virtually no longitudinal strain change is generated on the floor sensors. Conventional strain gauges, located near FBG array 1 show similar data.

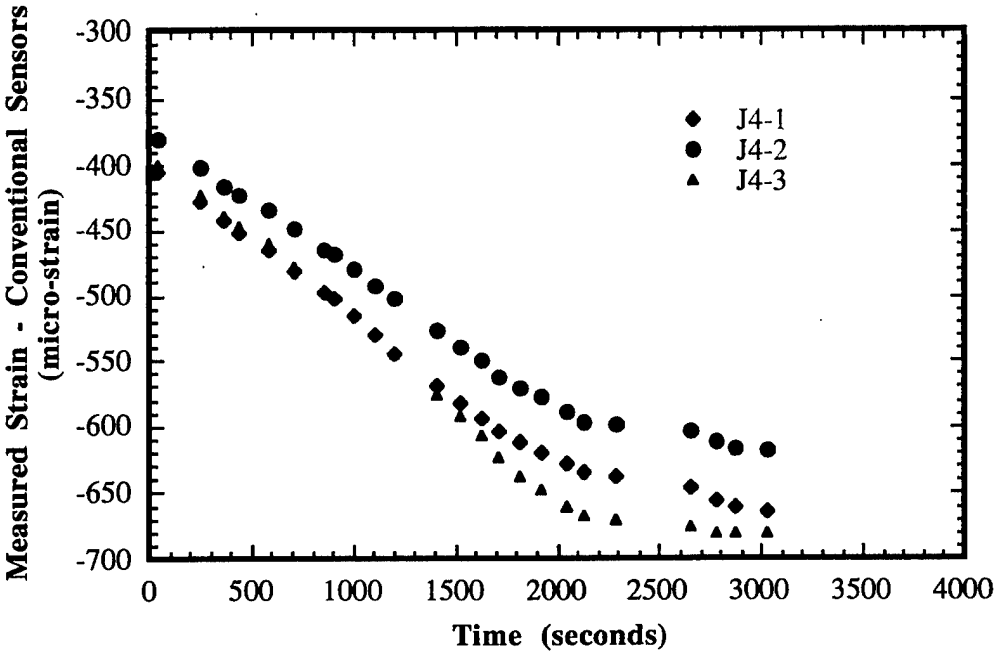

Figure 16. Strain data from conventional sensors located close to FBG array 1 during the same time frame as that of figure 15. Sensor J4-1 is close to the middle, J4-2 is close to the right and J4-3 is close to the left side of the floor (or flange) of the box-girder.

It should be noted that data from conventional gauges starts at approximately negative 400 micro-strain and increases in magnitude as the push continues. This is due to the fact that conventional gauges data were obtained from an absolute perspective while the Bragg grating data were obtained relative to a given measurement period. In other words, when the afternoon push phase started there was negative 400 micro-strain worth of compressive strain already present at the location of the sensors. In case of Bragg grating sensors, relative strain measurements were made, thus FBG data starts at zero strain and displays strain relative to zero starting strain for any given measurement

period. It is clear from Figures 15 and 16 that the strain response of the conventional gauges and Bragg grating gauges agrees quite well (apart from the –400 micro-strain offset). The relative strain measured by the two systems during the course of measurements agrees very well with each other. Both conventional and Bragg grating strain data show little change in the strain response once the sensor suites are directly over the pier, which seems to occur after about 3000 seconds. The shape of the data and the underlying mechanisms will be discussed in later sections. Next we apply a –400 micro-strain offset to Bragg grating data and compare it directly to conventional gauge data.

We have applied a strain offset of about 400 micro-strain to Bragg grating sensor data and compared them directly to conventional sensors in figure 17.

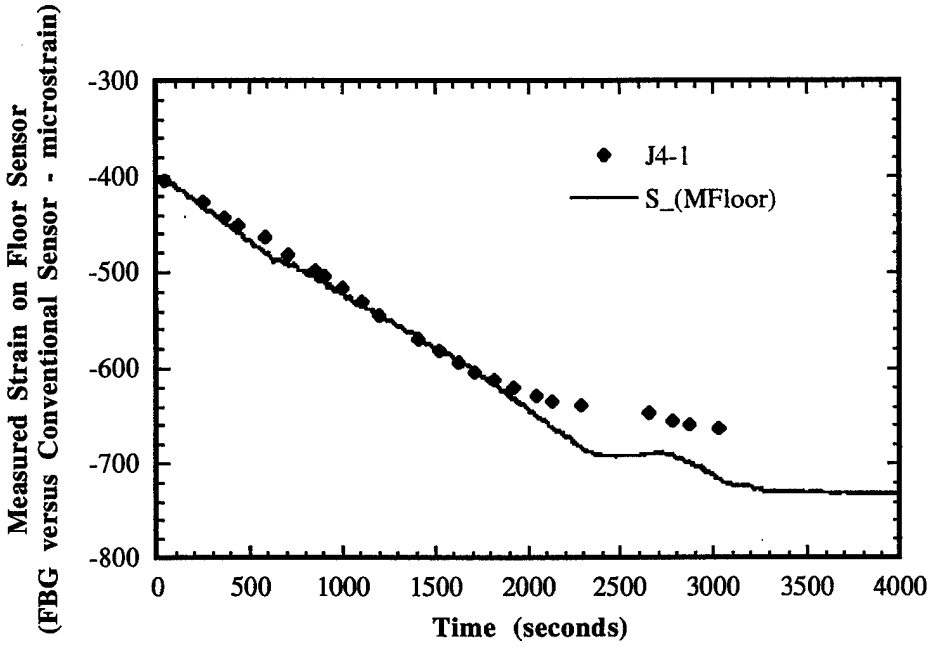

Figure 17. Data from a conventional and a Bragg grating sensor as recorded during the push beginning at 1:25 pm. Both sensors are located near the middle of the bottom flange (i.e. floor). The data is from region of the box-girder labeled FBG array1 in figure 8.

Direct comparison between conventional and FBG strain data clearly shows that the two agree quite well, especially for the first two thousand seconds. The reasons for departure from ideal match between the conventional and FBG sensors will be discussed after displaying data showing comparison between other conventional gauges and FBG sensors located on the floor. Appropriate strain offset to Bragg grating data from the left and right flange (i.e. floor) sensors was applied and compared directly to conventional sensors, as shown in Figures 19a and 19b.

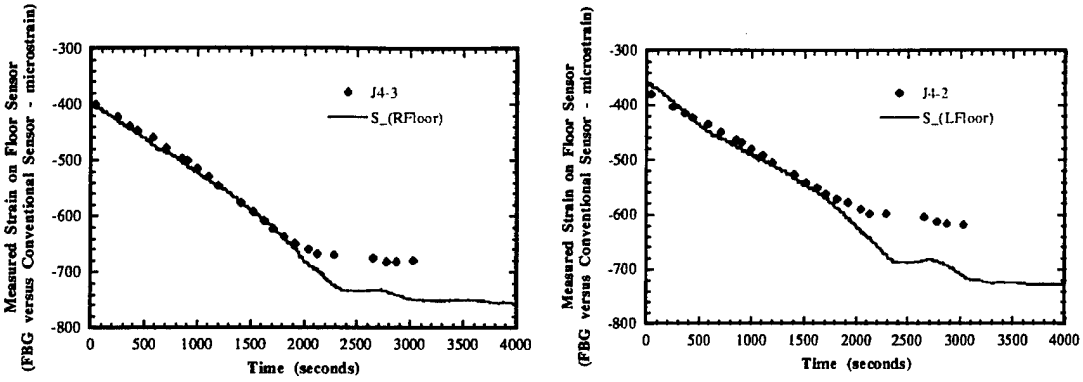

Figure 19. Data comparing conventional and Bragg grating sensors for the right (a) and the left (b) section of the box-girder of FBG array 1.

The data between the conventional and FBG gauges appear to agree quite well during the course of the launching starting at about 1:25 pm on February 4, 1998. The data agrees extremely well for the first 200 seconds of the push, however the conventional gauges data differs quantitatively by about 20% from the FBG data after the first 2000 seconds. Note that qualitatively the two data sets agree quite well with each other for all times. The conventional gauge data shows virtually no strain change after a certain time, as with the FBG sensor. However, the lack of strain change appears to happen earlier in time in the conventional gauge data while the FBG data continues to see compressive strains a little longer (see figures 17 and 18 near 2000 seconds). This is likely due to one of three reasons: (i) the conventional gauges were providing unreliable data, at certain times, according to EPFL-ICOM team in charge of conventional gauges, (ii) the conventional and Bragg grating sensors are not exactly co-located, in some cases the conventional and Bragg grating sensors are separated by as much as several centimeters and may be seeing different strains and (iii) the unknown role of local structural geometry and the lack of sensor co-location on the flange. The third point is elaborated further. Recall that there are stiffeners in the box-girder flange region. It turns out that the conventional gauges were located very close to the stiffeners, while the FBGs were located exactly in between the two stiffeners. Such a subtle difference in sensor location can be irrelevant when the sensor suite is away from the pier, as can be seen by the good agreement between the conventional and FBG data for the first 2000 seconds. However, as the region of the box-girder containing the sensors approaches the pier, the conventional sensors which are located closer to the stiffeners experience less strain than the FBG sensors which are located away from the stiffeners. In other words, this appears to be an effect driven by the details of the local structural design and the lack of exact co-location between conventional and FBG sensors.

8.4 Mathematical Model Describing the Push Phase:

The general features of the strain response curve shown in section 8.2 were modeled mathematically. The long cantilevered nature of the box-girder lends itself to modeling it as a beam, given that the dominant deflections occur in the vertical direction under the action of bending. Classical Euler-Bernoulli beam theory may be appropriate for such a system, but an improved theory based on a Timoshenko beam, which includes the effects of shear deformations, was utilized. The coupled shear-corrected equations describing the deflection of the beam are:

$$-EI\frac{\partial^2\Psi}{\partial x^2}+k_sGA(\Psi-\frac{\partial\Psi}{\partial x})=0 \qquad (1)$$

$$k_sGA(\frac{\partial\Psi}{\partial x}-\frac{\partial^2 w}{\partial x^2})=q(x).$$

Where w(x) is the vertical deflection, $\Psi(x)$ is the neutral axis rotation angle, k_s is the averaged shear coefficient, q(x) is the applied transverse load (the self-weight in this case), and E, G, I and A are girder geometric and material constants. The bending strain in the box-girder is given by

$$\varepsilon(x)=-z\frac{\partial\Psi}{\partial x}. \qquad (2)$$

Where z is the distance away from the neutral axis. The solution $\Psi(x)$ to equations (1), when inserted equations (2), is

$$\varepsilon(x)=\frac{ML^2z}{8EI}\left((x-1)(4x-12\kappa^2r^2-1)+e^2(6x-1)\right) \qquad (x<L)$$

$$=\frac{ML^2z}{8EI}4(1-x-e)^2 \qquad (x>L),$$

Where M=qL is the total mass of the box-girder, κ and r are non-dimensional parameters involving the geometric and materials constants, L is the distance between the second –to-last and last supports, and e is the length of the box-girder that is cantilevered beyond its last support. This result is shown in figure 19 where appropriate offsets in the theory are applied and the model compared directly to the data of one of the FBG sensors on the bottom flange (i.e. floor). The model predicts compressive strains in the flange followed by virtually no strain change as the box-girder is very close to the pier and directly over the pier.

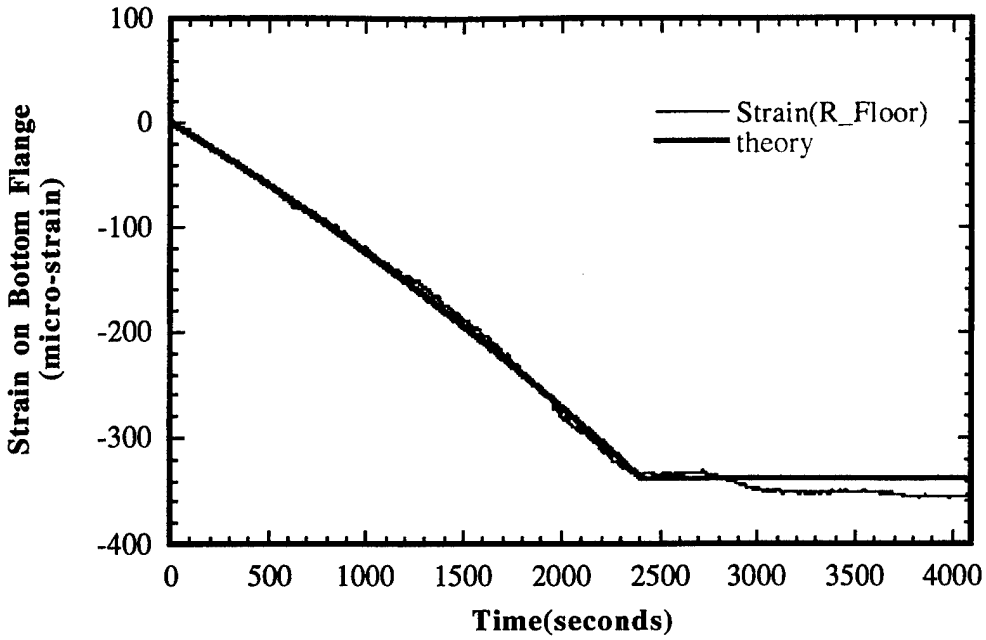

Figure 19. Comparison of the Timoshenko theory and experimental data from a Bragg grating sensor of FBG array 1 located on the bottom flange of box-girder bridge.

Figure 19 shows the data obtained from the box-girder bridge during the push phase of 1:25 pm and its agreement with the Timoshenko theory. The data from the theory is scaled appropriately to match the actual results obtained from the box-girder bridge. As mentioned earlier, the theory provides good qualitative agreement between the data from the sensors and the model. In order to obtain quantitative agreement between the field test data and the mathematical model, significant details regarding the box-girder structure are required which are currently unavailable. It should also be pointed out that the model represents a box-girder as a beam which, is a simplification and also does not consider stiffeners, the details of the box geometry, and the tapered box-girder design. Considering the simplifications, the model qualitatively agrees quite well with the observed strain data.

For completeness we are also depicting data from other sensors of FBG array 1 and FBG array 2 in figures 20-22. It should be noted that it is very difficult to provide a detailed description of the data from FBG array 2, which is located close to the cantilevered end of the box-girder. This is the 'free' end of the box-girder and tends to undergo very complex set of strain changes, displacements and even ultra low frequency oscillations. It is not easy to predict the motion or the subsequent strains induced near the of the free-end of the box-girder. However, for completeness the data from all the strain sensors are shown next. Notice that the sensors on the web, near the neutral axis show little strain magnitude (figures 20 and 21).

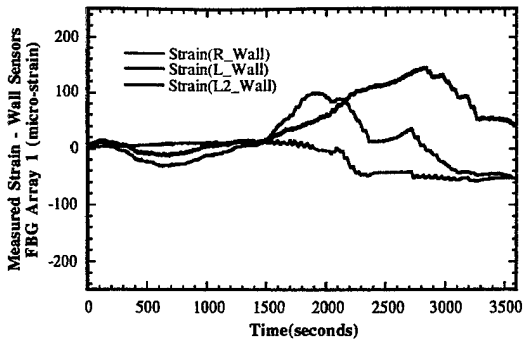

Figure 20. Measured response of the FBG sensors attached to the two webs (walls) of the box-girder structure. Data shows Bragg sensors from FBG array 1.

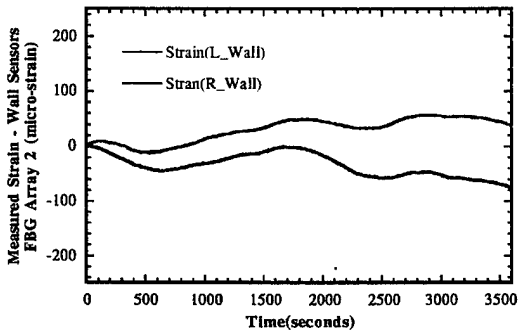

Figure 21. Measured response of the FBG sensors attached to the two webs (walls) of the box-girder structure. Data shows Bragg sensors from FBG array 1.

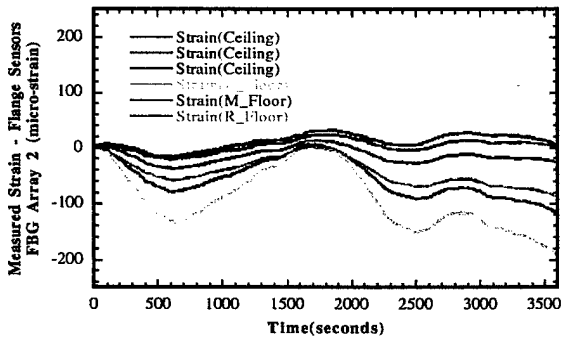

Figure 22 Response of the flange sensors of FBG array 2 (near the cantilevered end) during the push phase of 1:25 pm.

8.4 Data from the full push phase:

As has been mentioned before, the push occurred in several intervals and the response of the FBG arrays was monitored only during the actual times when the push was actually taking place. We have pieced together the data from various runs during the push phase of the box-girder on February 4, 1998. The data is shown as if the push took 140 minutes but it should be noted that the entire phase took about 8 hours while the actual launching occurred in intervals of 15 minutes to 55 minutes each. Data of figure 23 pieces together the measured FBG strain response from the various push phases, which took place on February 4, 1998. In total there are five time intervals during which significant push occurred on that day. In other words, the data shown in figure 23 represents the full push as measured using the FBG arrays after the data from all the relevant push intervals have been pieced together in to a single data set. The data shows that as the FBG array 1 approaches pier 1, the bottom flange of the box-girder tends to undergo compressive strains totaling almost 700 micro-strain. Such strain levels are considered no cause for alarm, however, keeping the strain history of the box-girder during construction is of importance from a design verification, safe operations and future maintenance perspective. This represents one of the first time such measurements are made in a distributed fashion on an in-construction box-girder structure and it represents the first time that such strain profiling is done with wavelength division multiplexed (WDM) arrays of fiber Bragg grating sensors on an in-construction box-girder bridge. The result show excellent promise for using WDM fiber strain sensor systems on civilian infrastructure.

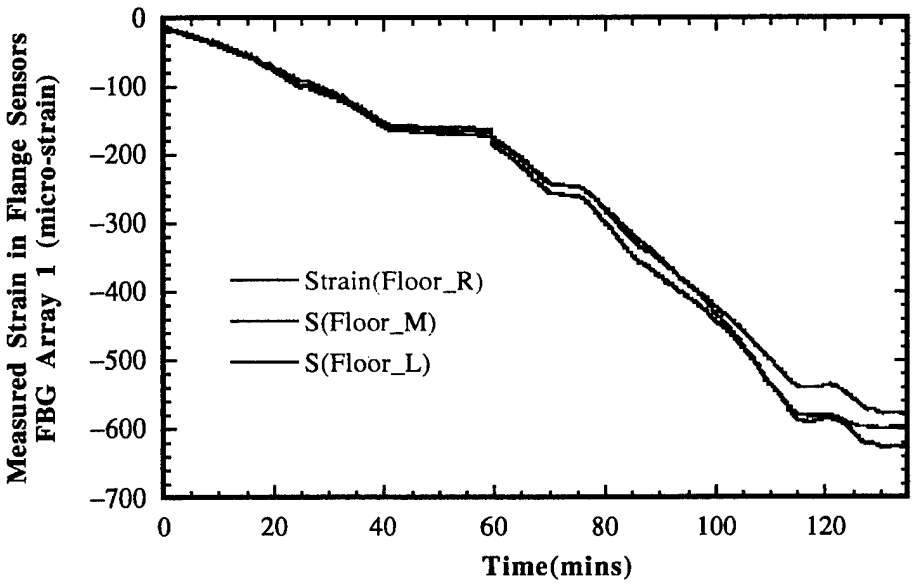

Figure 23. Measured Bragg grating strain data from sensors located on the bottom flange (i.e. floor). The data is from box-girder location marked FBG array 1 in figure 6 and covers the full push phase which started at around 9 am on February 4, 1998. The data represents a total push of about 25 meters from about 9 am to about 3 pm.

The push represents a total travel distance of the box-girder of approximately 25 meters. For completeness we also show data from FBG sensors other than the ones located on the bottom flange of FBG array 1, though the sensors at the bottom flange do represent the highest strain recorded during this particular push phase. Figure 25 shows data from the web sensors (i.e. sensors on the left and right walls of the box-girder) of FBG array 1. Figures 25 and 26 show data from all the strain sensors located in FBG array 2. Not surprisingly the data from sensors located on the webs (i.e. walls) of FBG array 1 and array 2 had the potential to be quite interesting, however due to the fact that they were attached so close to the neutral axis renders them uninteresting providing not very useful strain data. The flange sensors (i.e. the sensors located on the floor as well as the ceiling) of FBG array 2 show slightly more interesting data, however, this array is too close to the free end of the box-girder which tends to undergo very complex strain changes due to local effects from low frequency oscillations of the free-end, curvature of the terrain and the local complexities of the box-girder structure. However, for completeness, data from all the strain sensors are shown in figures 24-26 for the push phase from 9 am to about 3 pm on February 4, 1998.

The strain data as measured during the push phase of February 4, 1998 at two separate locations of the box-girder bridge are shown in figures 24-26. As seen in figure 23, strains of greater than 500 micro-strain can be observed on the flange sensors (i.e. floor sensors) of FBG array 1. This is expected since the flange sensors are located such that as that part of the box-girder approaches pier 1 during the launching, it tends to produce substantial compressive loads resulting in negative strains in the flange (i.e. floor sensors. On the other hand, the flange sensors of FBG array 2, which is located near the cantilevered end of the box-girder do not see large strains. The web sensors of both FBG sensors, which are all unfortunately located close to the neutral axis of the box-girder tend to show very little strain, as expected. At the time of sensor attachment the precise location of the neutral axis of the box-girder was unclear. Since the FBGs on the web were attached longitudinally, little strain is expected in the longitudinal direction as is evidenced by the data from figure 24 and 26. However, as is also clear the strain on the web sensors is not zero. This is due to the fact that the sensors are located close to the neutral axis and the exact location of the neutral axis is unknown. Some localized strain effects can be seen in some of the web sensors (figure 24, left web sensor), especially as the sensor is directly over the pier. Such effects are absent in the web sensors of FBG array 2 since that array is at the free end of the cantilever and does not see local effects from vertical loading from a pier.

Next, we discuss the results from the 'pull-up' phase of construction. This is the phase, which occurs immediately after the push phase and actually involves lifting the cantilevered end of the box-girder on to the far pier. This induced substantial strains at various locations on the structure. The pull-up phase was monitored with the FBG strain sensors and also in limited case with conventional resistive strain gauges.

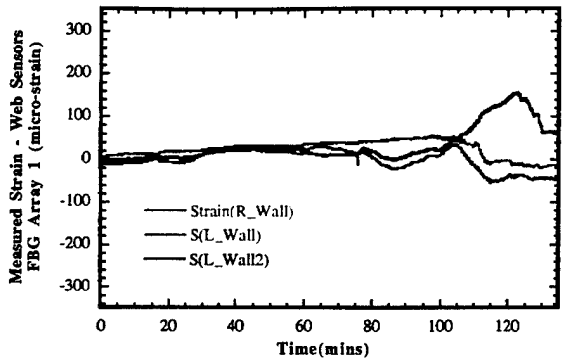

Figure 24. Measured Bragg grating strain data from sensors located on the web (i.e. walls). The data is from the box-girder location marked FBG array 1 in figure 8 and covers the full push phase which started at around 9 am on February 4, 1998.

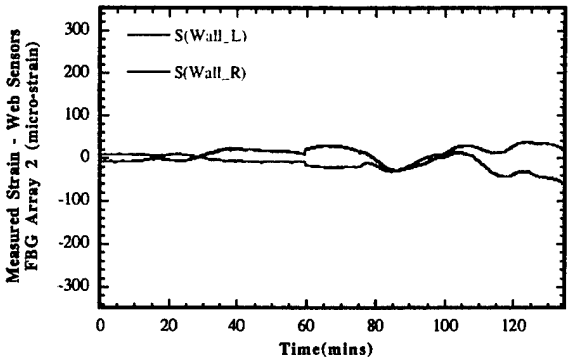

Figure 25. Measured Bragg grating strain data from sensors located on the flange (i.e. floor). The data is from the box-girder location marked FBG array 2 in figure 8.

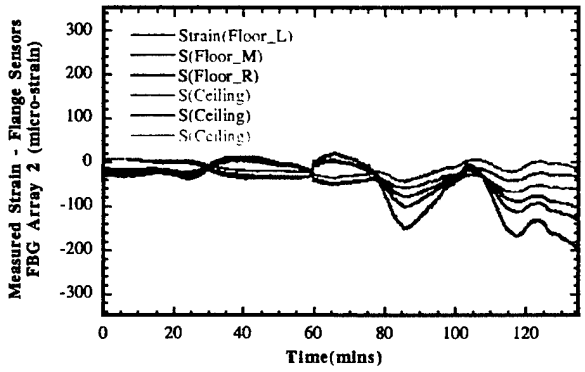

Figure 26. Measured Bragg grating strain data from sensors located on the web (i.e. wall). The data is from the box-girder location marked FBG array 2 in figure 8.

9. Measurements During the Pull-Up Phase of the Box-Girder (February 4, 1998):

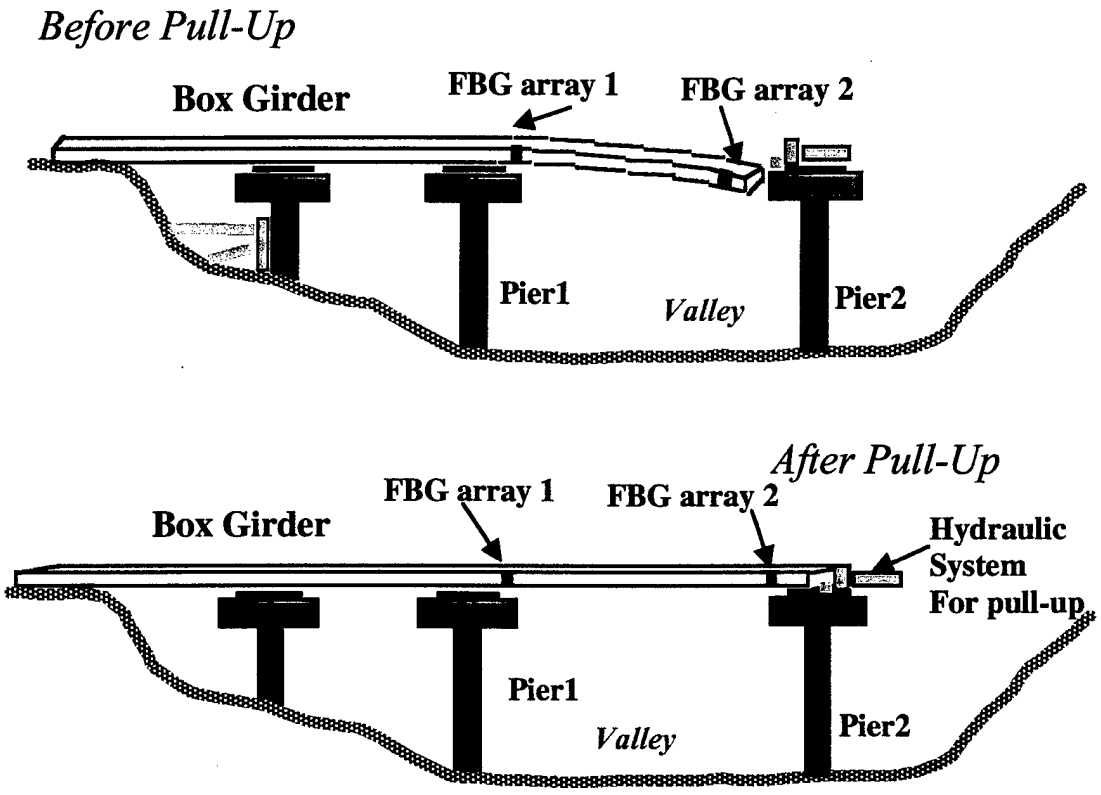

Figure 27. Schematic depicting the position of the box-girder before (top) and after (bottom) of the pull-up phase.

9.1 Introduction:

A schematic of the box-girder depicts the position of the box-girder immediately after the push from pier 1 to pier 2 in figure 29 (top), where the box-girder has assumed a cantilevered position. The construction process at this stage involves attaching the free-end of the box-girder to a hydraulic system, which pulls it up such that it is no longer in cantilevered position. The box-girder at this stage does not have a free-end and is no longer cantilevered. This is followed by a small push of the box-girder on to pier 2 where it is allowed to rest (figure 27 – bottom) until the next phase of construction. In this section of the report we will discuss the strains incurred by the box-girder at the two locations which are instrumented with strain sensors. Primarily, we will describe the strains incurred at locations labeled, FBG array 1 and FBG array 2, as the hydraulic system picks up the box-girder from its cantilevered position. There should be significant strains incurred at both locations and we will compare Bragg grating data to conventional gauge data where possible. Again, we do not expect significant strains on the web (or the wall) sensors of either array as they are too close to the neutral axis of the structure.

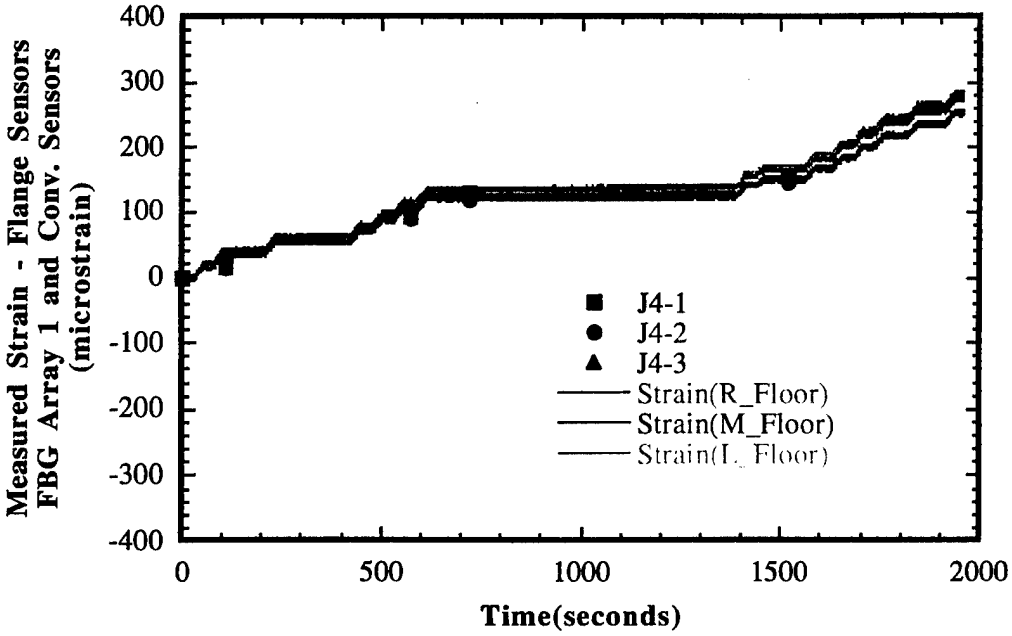

Figure 28. Measured data from the three flange sensors (floor) of FBG array 1 during the pull-up phase of construction on February 4, 1998. Corresponding conventional sensor data is also show.

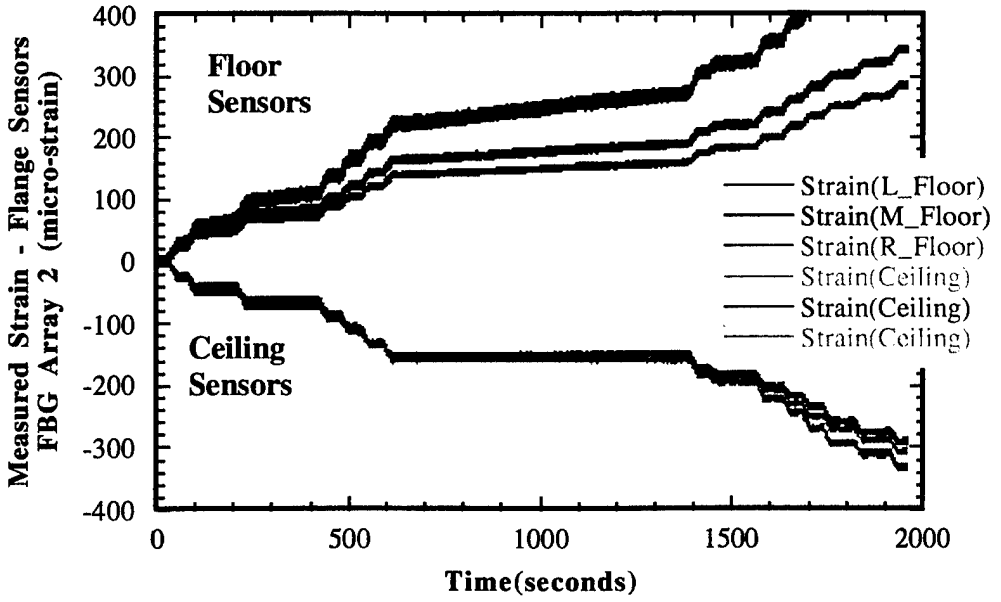

Figure 29. Measured data from the six flange sensors (three on floor, three on ceiling) from FBG array 2 during the pull-up phase of construction on February 4, 1998.

9.2 Data from Pull-Up Phase of February 4, 1998:

As can be seen from figures 28 and 29 substantial strains are generated at locations of the two FBG arrays during the pull-up process. The data of figure 28 and 29 starts off at zero strain since the Fabry-Perot reading unit starts all new data runs in that manner, as explained in an earlier section. Therefore, all data shown is relative strain data. Also as a reminder, FBG array 1 did not have any sensors on the ceiling thus the data from the flange region consists of floor (or bottom flange) sensor data only as can be seen in figure 328. On the other hand, both the top and bottom flange regions of FBG array 2 have optical strain sensors on it thus providing us with data from both the ceiling and the floor during the pull-up phase. In addition, we show data from conventional gauges which are located near FBG array 1 and compare its response directly to the response of FBG sensors during the pull-up process (figure 328). Conventional gauges situated near FBG array 2 were not activated during the pull-up phase and so comparison between sensor data from FBG array 2 and conventional gauges is not possible.

The actual pull-up seems to have occurred in a step like motion as the data of both figures 28 and 29 indicate. There also seems to have been a long pause into the pull-up phase between 600 and 1400 seconds. Such pauses are common, as the construction crew inspects the progress of the pull-up phase and makes adjustments, which might be necessary. The strain magnitude reaches above 300 micro-strain in all flange sensors. As expected, the strain response from the floor and the ceiling should have opposite signs as is evidenced by the data in figure 29. When the floor sensors undergo tension and induce positive longitudinal strain, the ceiling sensors do the opposite. One would expect strains from the ceiling and floor strain sensors to be equal in magnitude and opposite in sign. However, the physical layout of the terrain and the bridge design is such that the box-girder curves in a given direction thus breaking the symmetry which, would have allowed for the floor and ceiling sensors to have exactly equal magnitude. Additionally, the fact that the hydraulic system may not be attached to the box-girder such that it induces uniform strain at all three locations of the bottom flange sensors, it is likely to be responsible for providing strains of slightly different magnitude in the three bottom flange sensors of FBG array 2 as is shown in figure 29. However, considering the complexity of the details of the box-girder design, the terrain and the local geometrical effects, the strain data during the pull-up phase is as expected.

For completeness, data from the web (i.e. wall) sensors during the pull-up phase is shown in figure 30. Not surprisingly little strain is induced in the web sensors which were attached very close to the neutral axis of the box-girder, as mentioned earlier. For comparison, data from one of the flange sensors is shown along with data from all the web sensors which highlights that strain magnitude is quite small in the web sensors, as expected. It should be noticed in the data of figures 28-30 that there is substantial 'fuzz' in the data from all sensors during the pull-up phase. The data 'fuzz' appears to be quite large, on the order of about $\pm$ 7 micro-strain. It would appear that this is indicative of increased noise in the strain sensing system. However, closer inspection reveals that this 'fuzz' is due to the pumps in the hydraulic system responsible for pulling up the box-girder from its cantilevered position. The pump tends to generate sound waves which manifest themselves through the structure and produces small dynamic strain in the entire box-girder.

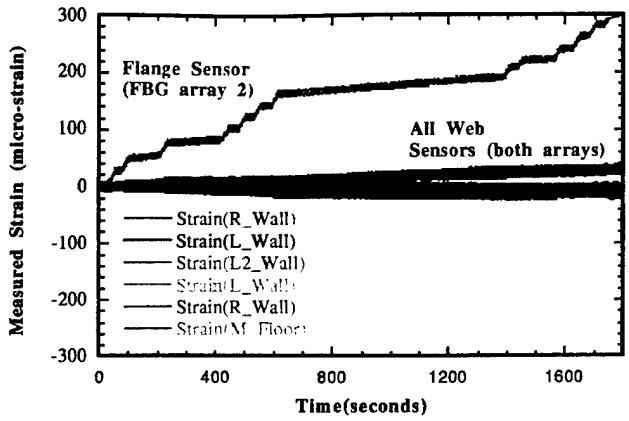

Figure 30. Comparison of strain in the web and flange during the pull-up.

Since the optical strain sensing system is sampling data at a rate of 2 Hz, this vibration is detected by the FBG system. On the other hand, the conventional system records data at discrete intervals (in some cases every 10 minutes) and is unable to measure any dynamical effects.

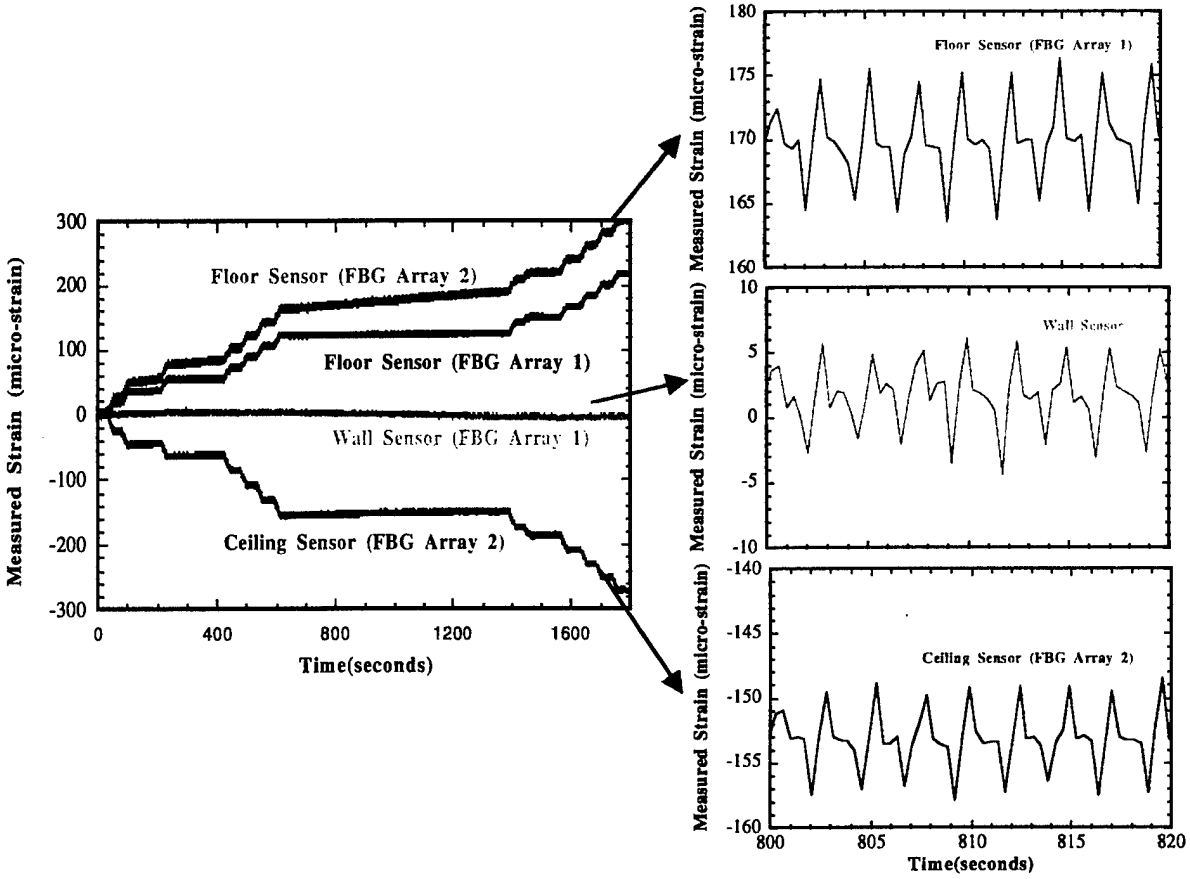

Figure 31. Vibrational response of hydraulic system measured by the FBG arrays.

The vibrational response of the bridge due to the attached hydraulic pump system is shown in figure 31 for FBG sensors from three locations. All three locations show the same vibrational response with a period of about 2.3 seconds indicating that this is not a local effect but an induced vibration due to external effects, like the hydraulic pump, propagating through out the box-girder structure. Potential benefits of such data could be in developing advanced forms of structural integrity assessment techniques including detection of localized deformities and damage by exciting the structure dynamically.

Finally, we display data from the full phase of the test, which took place on February 4, 1998. This includes the push data as well as the pull-up data pieced together in such a way that it shows the history of strain at the location of the box-girder which we have labeled FBG array 1 in figure 6.

10. Strain history at two locations of the box-girder:

Figure 32 shows that the data from the entire test (push + pull-up phases), which took place on February 4, 1998. The data includes both the push and pull-up phases. The data in figure 32, provides a good indication of the magnitude and sign of the strain changes the structure is undergoing during the entire launch and recovery phase of February 4, 1998. Unfortunately, the clocks of the two data collection systems (FBG optical sensors and conventional sensors) are not synchronized sufficiently to allow for direct comparison between the two data sets on a single graph. Therefore, FBG array data and conventional gauge data are shown on separate graphs (figure 34 and 35). Additionally, conventional strains gauges were not activated before 10 am while FBG arrays started collecting data at 9:10 am on the day of the push. This complicates direct comparison for the full phase even further. These difficulties are alleviated when comparing only sort segments of the data runs as done in previous sections. In figures 32 and 33 we display data as obtained from the clock settings of the individual systems.

FBG array data was pieced together from four files ranging between 10 minutes and 55 minutes, thus the total time length is on the order of 175 minutes. Conventional gauges, on the other hand took data at discrete times. This lack of synchronization between the two time clocks requires interpretation of the two data sets further. Despite this lack of synchronicity between the data collection systems, there are obvious common features within the data. The push phase is clearly identified as providing compressive loads on the flange while the pull-up phase provide tension in the flange, as is evidenced in figures 32 and 33. The approach of the box-girder structure towards the pier provides compressive loads but as the structure is just prior to or directly above the pier, it results in virtually no strain change in the flange as is seen in both sensor types. Comparing magnitude of strain change as recorded by the two sensor systems it is obvious that the magnitudes match very well if one compare them fairly and carefully. For instance, the relative strain as recorded by the FBG gauge between minutes 40 and 120 is about 425 micro-strain. Similarly , the relative strain as recorded by the conventional gauges between minutes 40 and 300 is approximately 410 micro-strain, which is quite close to that measured by the FBG array. Again, due to time synchronization discrepancies and the fact that conventional gauges did not start recording data until 40 minutes after the FBG arrays, such seemingly unusual time scale comparisons have to be invoked in order to properly interpret the data.

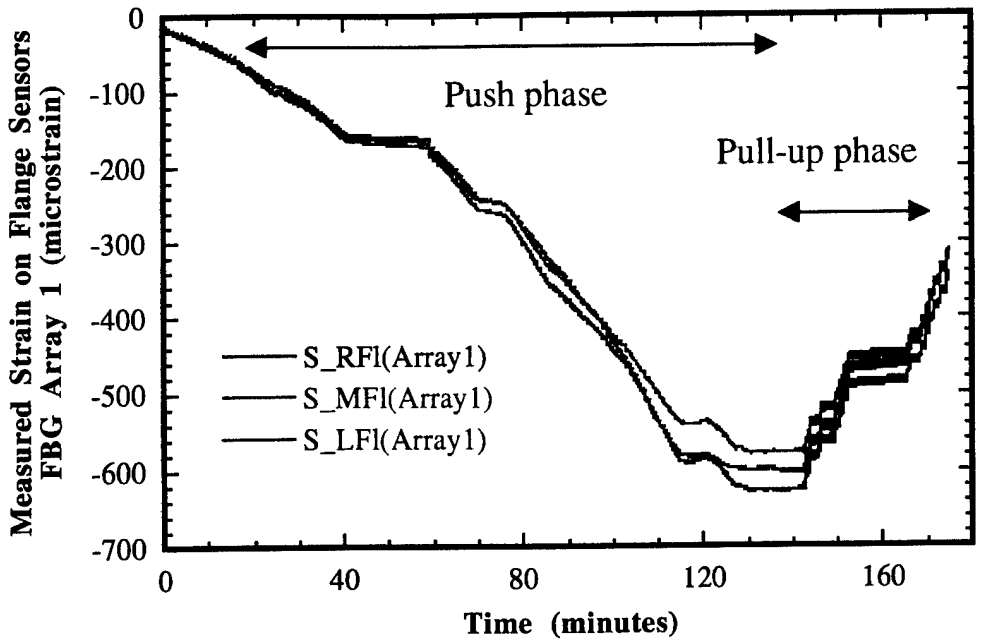

Figure 32. Data from the bottom flange sensors of the FBG array 1 for the full push.

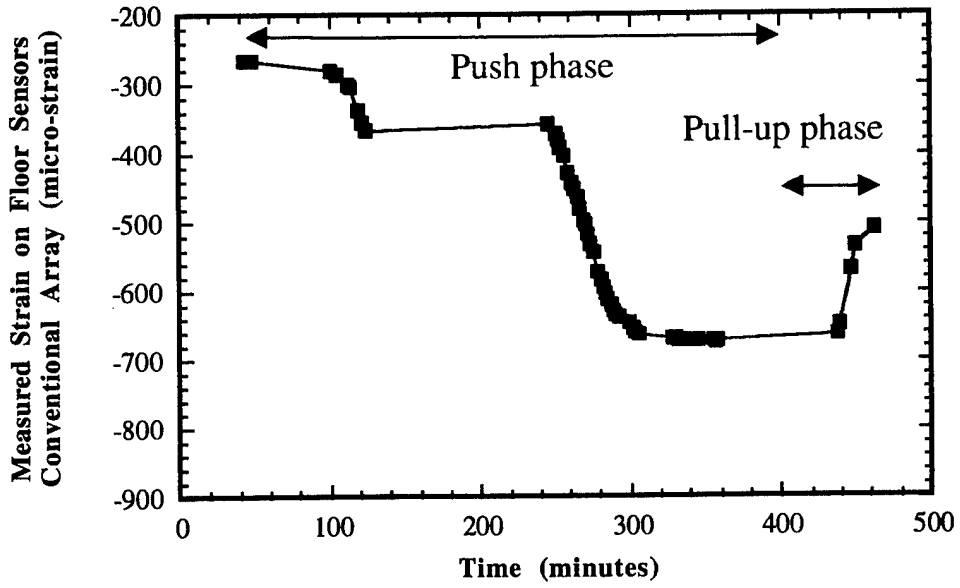

Figure 33. Data from bottom flange sensors of conventional array for the full test.

11. Measurements During the October 27, 1998 Push of Box-Girder:

11.1 Introduction:

After the push phase of February 1998, the construction involved completing one direction of the bridge by building a concrete deck on top of the box-girder structure. This phase of construction process took place during spring and summer of 1998. NRL team was not present during any of those phases of construction. In early fall, construction of the second box-girder to carry traffic in the opposite direction began in earnest. It was decided that NRL should try and make further strain measurements on the second box-girder structure. The lessons learned during the tests of February 1998 were expected to help in determining better sensor location and in obtaining more variety in strain measurements. For instance, while attaching gratings in the longitudinal direction close to the neutral axis yielded little useful information during the February test, it was pointed out that attaching gratings in the vertical and diagonal direction on the web of the box-girder could yield invaluable information regarding any localized buckling which might be taking place during the push phase. As mentioned in the introduction of this work, localized buckling of the web is of critical importance during construction since it can cause catastrophic damage and millions of dollars worth of expenses. As usual, the EPFL-ICOM team was also going to be making measurements at various locations. Additionally, novel Bragg grating based concrete embeddable sensors were also being tried during this field test. The results of the concrete embedded sensor test will be described in another report.

The chosen location for attaching the FBG sensors was inside the box-girder at a place which was about seven meters away from a given pier over which the push was to occur. The push was expected to be such that the region of the box-girder with the sensor suite was to travel over the pier and about ten meters beyond the pier. In other words, during this test we should be able to make strain measurements such that we have symmetric strain data from either side of the pier. Additionally, the plan was to attach sensors longitudinally, vertically and diagonally at the chosen location in order to obtain multi-axis strain measurements in the box-girder. We also chose fewer gratings for measuring the temperature of the structure. Heat sink compound was not used to thermally attach the gratings. All together, twelve gratings were used during this push phase. The grating interrogation was done similarly to the way in which it was done during the February test. The grating attachment method was also very similar. The main differences were in the way in which the temperature gratings were attached to the structure and the exact orientation of the sensors.

11.2 Sensor Attachment:

The gratings meant for measuring structural strain were attached to the box-girder using the method described in earlier section. The gratings meant for measuring the temperature of the structure were placed loosely inside a small brass tube (2 4 cm x 3 mm diameter) and the tube bonded to the structure. Thermal changes on the structure would be transmitted to the brass tube and only the thermal component would be sensed by the grating since it is loosely placed inside the brass tube. This approach seemed to work considerably better than the approach attempted during the February test. Temperature of

the structure was measured only in two locations and the rest of the gratings were used for strain measurements.

11.3 Sensor locations and Orientation:

Bragg grating sensors were located inside the box-girder at a location which was about seven meters away from a given pier over which the push was to take place. It was expected that the location would travel over the pier and on to the other side of the pier for about ten meter. Since this test was primarily meant to measure the effects of the vertical loading provided by the pier to the web region of the box-girder, strain sensors were attached on one side wall (i.e. web) of the box-girder.

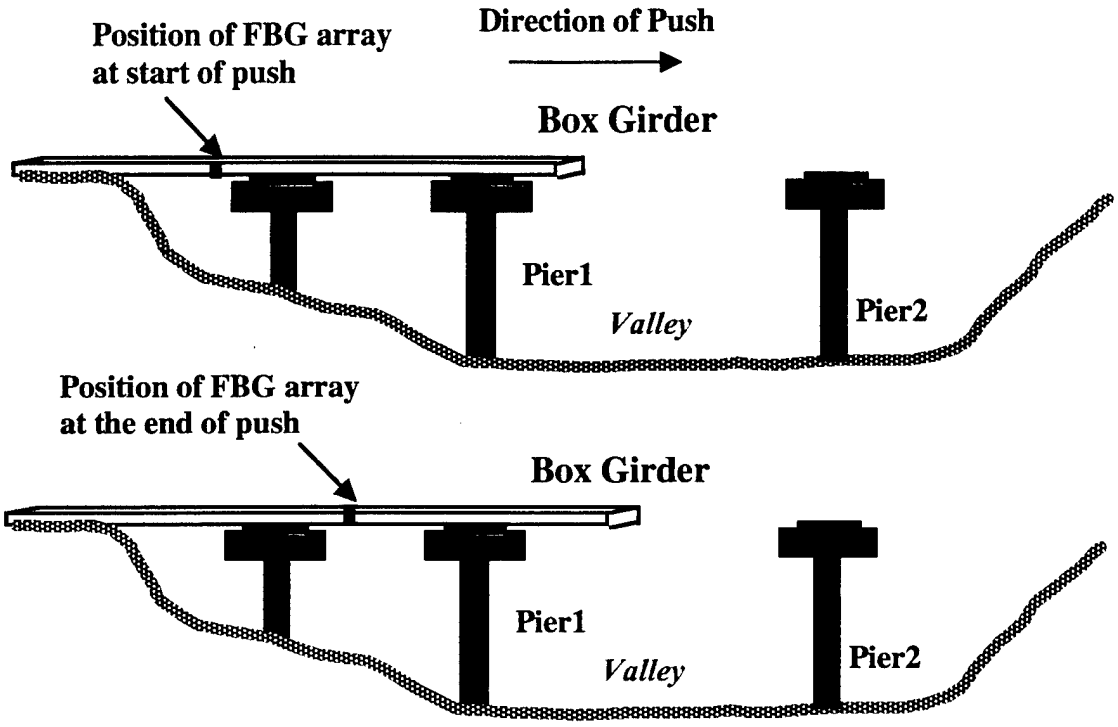

Figure 34. Schematic showing the position of the FBG array before (top) and after (bottom) the push of October 1998. The total travel was expected to be between 17 and 20 meters from the original point of the sensor location. The location of the Bragg grating array was about seven meters away from the pier prior to the push.

As defined by the construction foreman, this would be considered a small push. A big push would be defined by the kind of push we measured during February 1998 which involves cantilevering of the box-girder followed by the pull-up phase. However, since we are primarily interested in the local phenomena due to the vertical loading induced by the pier on the box-girder web, the travel distance of the push was only important to the extent that it provide symmetric vertical loading during the push phase.

Majority of the strain gratings in the array were attached on one wall (i.e. web) of the box-girder with a couple on the floor (i.e. flange) for comparing the effect of vertical

reactions of the on the web and the flange. Sensors were oriented in the vertical, longitudinal and diagonal direction as shown in figure 35. Unfortunately, conventional sensor wre located far away from the Bragg grating array.

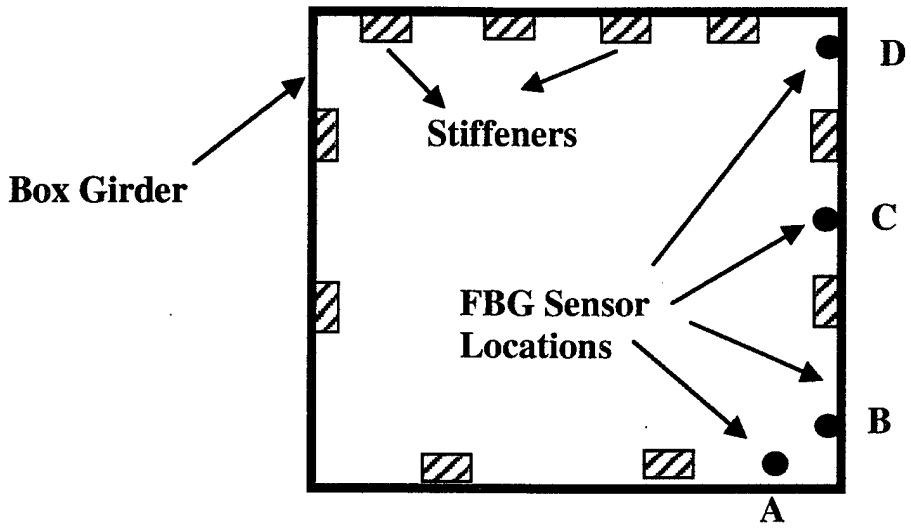

Figure 35. Cross-section of the box-girder showing the position of the stiffeners and fiber Bragg grating sensors.

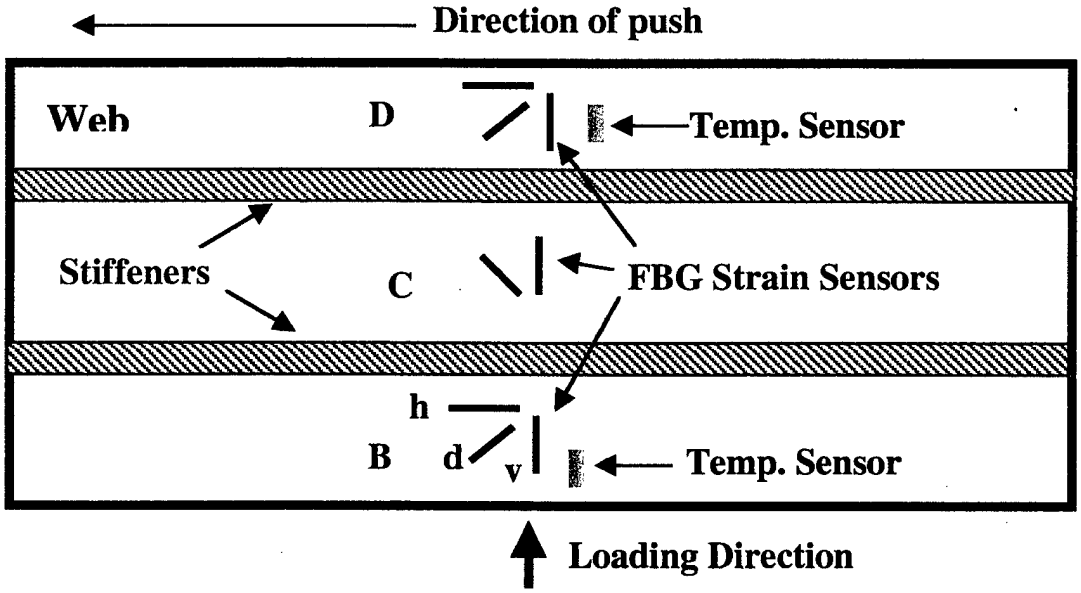

Figure 36. Schematic showing the orientation of the FBG sensors attached on the web (or the wall) of the box-girder, as would appear if looking at it directly. The relative positions of the sensors to the stiffeners on the web is also shown. Sensor locations B and D have three FBG strain sensors (vertical, diagonal and horizontal) plus a temperature sensor each. Sensor location C only has diagonally and vertically oriented sensors.

Orientation of the FBG strain sensors on one of the webs (or the wall) of the box-girder is shown in figure 36. A rosette type orientation can be seen in the top and bottom

three sensors attached to the wall. There is no longitudinally oriented sensor at location C for the simple reason that it is close to the neutral axis of the box-girder and little or no strain in that direction is expected. However, we expect strains in the vertical direction due to vertical loading of the web as it passes over the pier. Two Bragg grating sensors (one longitudinally the other diagonally) are also attached on the flange near the corner of the web and flange (sensor location A), as described in figure 35. The purpose behind choosing the flange sensor location was to determine the magnitude of the effects of vertical loading, especially the effects of the web buckling on the flange. In addition, two Bragg gratings configured to measure temperature are also mounted as described earlier, one at the top and the other at the bottom of the web as shown in figure 36.

11.4 Results from the push phase (October 1998):

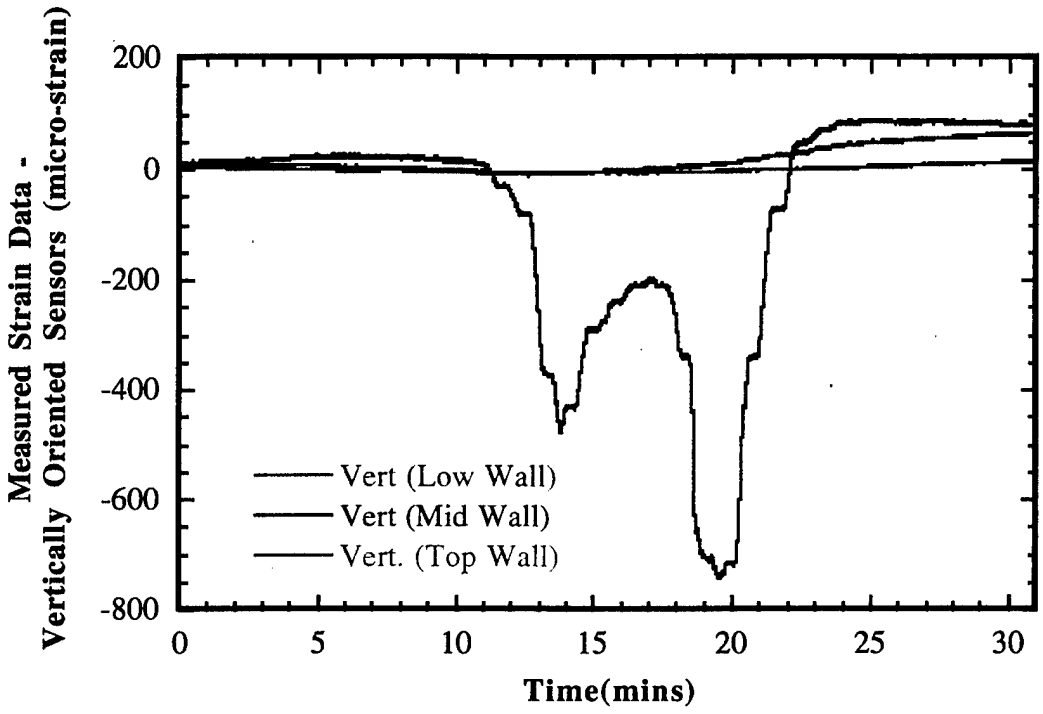

Figure 37. Data from the three vertically oriented Bragg grating strain sensors attached to the bottom, middle and top of the web. Compressive strains indicate the web was buckling outwards since the sensors are attached on the inside wall.

The data shown in figure 37 is fairly remarkable. Very large strain levels are observed in the vertically oriented FBG sensor attached to the lower web (from sensor suite B) as the box-girder approaches the pier, passes directly over the pier and then goes past it. The other two vertically oriented sensors, one in the middle of the web (from sensor suite C) and one on the top (from sensor suite D) do not show significant strains. The large strain levels observed in the vertically oriented sensor located on the lower web is a direct result of the 'localized' buckling of that region due to vertical forces induced

by the pier as the box-girder passes over it. It is precisely this type of localized buckling in the structure, which is worth monitoring. As is clear from the data of figure 37, the buckling is within the elastic limit of the structure since the structure returns to its original state after the reactive forces have been removed. In other words, the lower web of the box-girder undergoes buckling from vertical loading as it passes over the pier but returns to its unbuckled state after traveling past the pier. If this were not the case it would be cause for alarm and construction may have to be halted in order to repair that region. Additionally, it is also clear that the vertical loading provided by the pier is confined to the bottom part of the web and does not 'propagate' toward the middle or the top of the web. This is because the stiffeners play a substantial load in reducing the reactive forces from affecting other parts of the web. In other words, the box-girder design is good and is able to withstand simple elastic buckling loads in the local region. The effect is schematically summarized in figure 38 and qualitatively modeled with a simple equation in the next section. The precise shape of the buckling curve ('W'-shaped curve shown in figure 37) will also be explained in the next section.

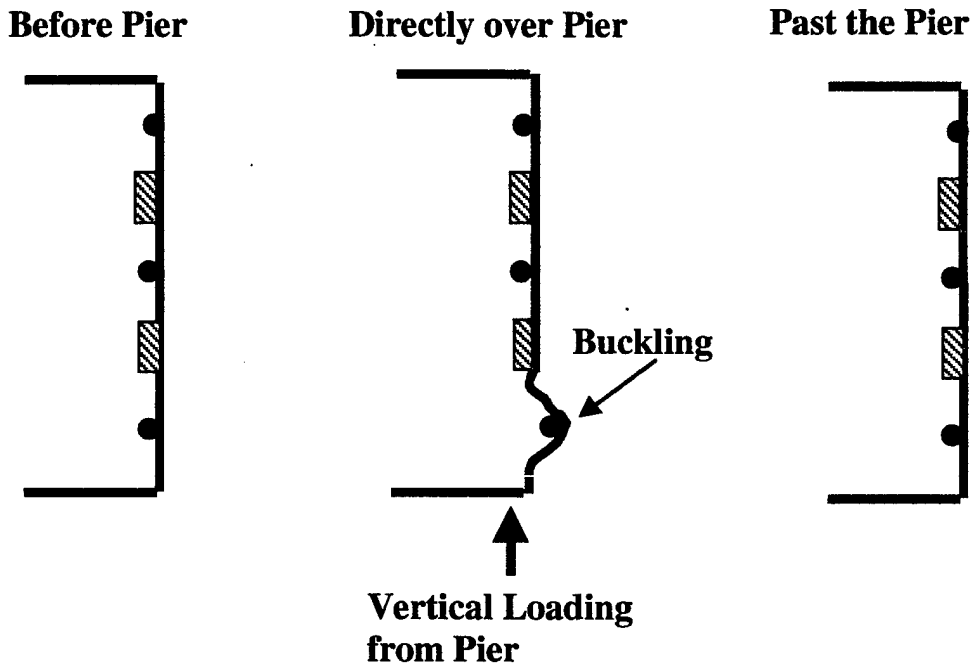

Figure 38. Schematic showing buckling of the lower web of the box-girder as it travels over the pier. The shown buckling is exaggerated. Based on the data of figure 37 it is clear that the buckling is confined to the lower web and the stiffeners play a significant role in not allowing the web to buckle beyond the lower part of the web.

11.5 Discussion on the Buckling Effect of Lower Web:

Since the buckling of the lower web is a localized phenomena we can model it by using a simple structural buckling of beams and plates model. A second approach which

could be used to explain the shape of the buckling curve is by using the approach of bifurcation theory. A pitchfork bifurcation equation can provide a better insight into the physical problem. In bifurcation theory, a pitchfork bifurcation can be described by the following equation (sometimes also known as a normal form),

$$(\partial x/\partial t) = rx - x^3$$

Note that the equation is invariant under the change of variable x to –x. This signifies that the buckling of the beam can occur to the left or right under critical loads. The parameter r represents the magnitude of the critical load, which is our case also means the distance traveled by the box-girder. A simple analysis of the equation reveals that it has one stable solution for $r < 0$, namely $x = 0$. In other words, there is no buckling of the beam prior to any influence of reactive forces. As r approaches and become greater than zero, the original stability point, namely $x = 0$, becomes unstable and gives rise to two new stability branches, namely $x = \pm \sqrt{r}$. In simpler terms, this means that when the beam is away from the influences of vertical loading it is unbuckled and as vertical loading influence increases, the beam undergoes buckling. Whether it buckles to the left or the right (i.e. mathematically $+\sqrt{r}$ or the $-\sqrt{r}$ branch of the solution is picked) depends on local conditions. As the vertical influence decreases, the solution traces itself back on the same branch of solution it took and goes through $r = 0$ where the unbuckled solution is obtained again. This is shown in figure 39 along with the state of the buckled beam.

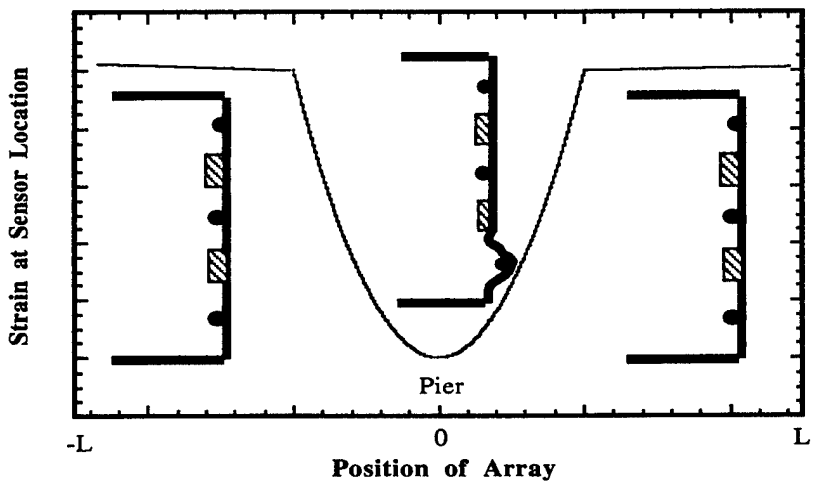

Figure 39. A qualitative curve showing the predicted strain in the vertical direction of the web as a function of the array position as the box-girder passes over the pier. The qualitative curve is based on equation (4). The approximate physical state of the box-girder is also shown.

It can be immediately noticed that the predicted curve of the strain response is different from the measured response (figure 37), especially in the middle where the

measured curve shows a sudden decrease in strain followed by a turn around, further increase in strain magnitude and then a continuous decrease in the strain magnitude. In other words, the predicted curve agrees with the measured curve except in the middle. This phenomenon is explained as follows.

When the box-girder is pushed a sliding shoe is used on the pier in order to reduce friction and provide a smooth slide. The sliding shoe is expected to be flat such that the box-girder is assumed to make contact with it at all times while sliding over it. However, sliding shoes are not perfectly flat and occasionally tend to have a curved surface. This is illustrated in figure 40 below.

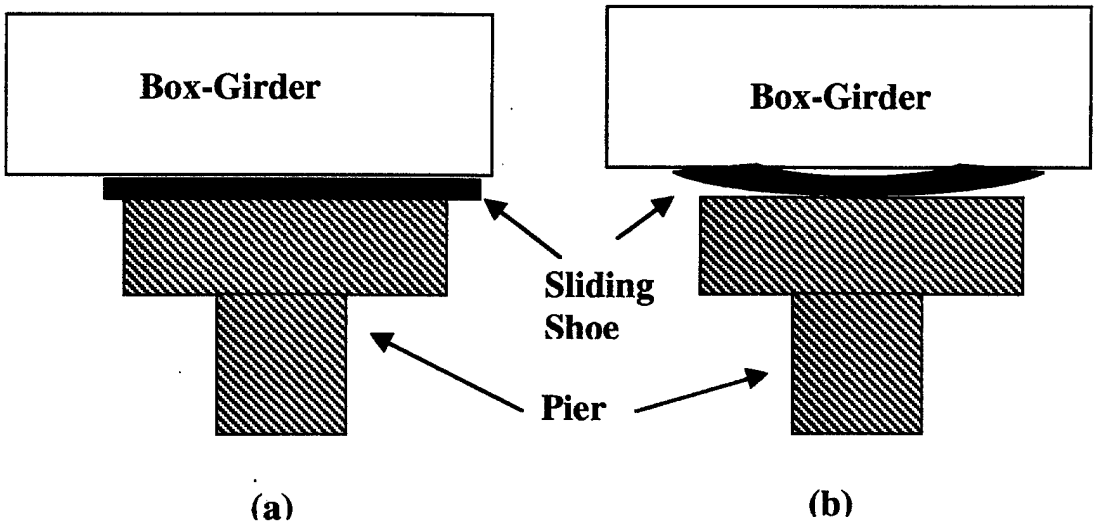

Figure 40 A schematic showing the vertical loading influence of an (a) ideally shaped and (b) curved shaped sliding shoe over which the box-girder slides during the push phase. The curvature may be exaggerated for illustrative purposes.

As can be conjectured from the illustration of figure 40, the vertical loading will be slightly different in case of a curved sliding-shoe than for a flat sliding-shoe. In case of the curved sliding shoe the magnitude of the vertical reactions will be reduced when the box-girder is not making perfect contact with the sliding-shoe as would be the case in the middle part. This reduction in contact between the sliding shoe and the box-girder, especially in the middle portion of the sliding shoe, leads to reduced vertical loading resulting in the abrupt change in strain magnitude in the middle of the measured curve of figure 37. Since this effect is a result of 'imperfections' in construction process, it is difficult predict this effect ahead of time.

Conventional strain gauges attached on lower web have shown very similar data sets. Even though no conventional gauges were co-located with the FBG array for this test, we expect to see very similar data sets from other push phases where conventional gauges were attached to the lower web in the vertical direction. As mentioned earlier, the

buckling of the web is a local phenomenon and should be observed at other times with similar magnitude strain and shape for lower web, middle web and top web regions.

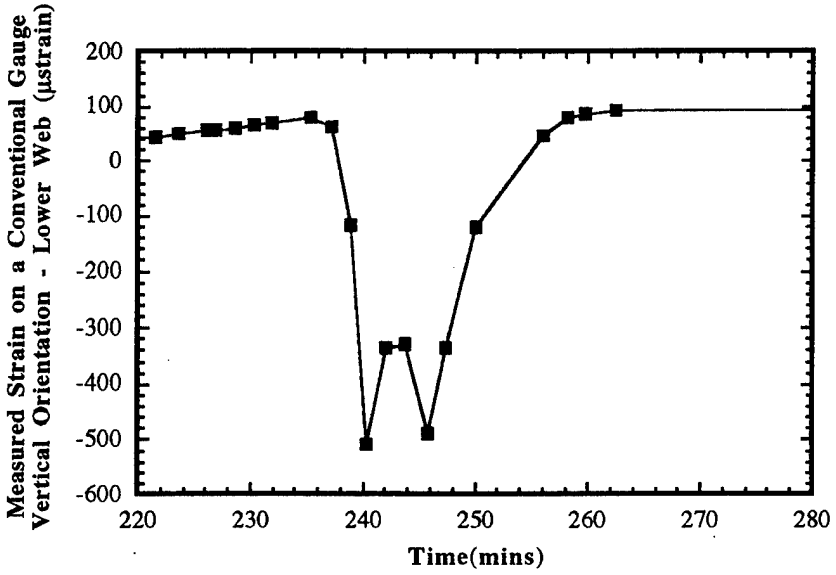

Figure 41. Strain data from a vertically conventional strain gauge located on the lower web of the box-girder, as the box-girder passes over the sliding shoe.

Strain data of figure 41 shows the response of a vertically oriented conventional strain gauge located on the lower web. The data is taken as the box-girder passes over the pier. Vertical loading buckles the web, which induces compressive strain on the lower web. The curved shape of the sliding shoe is responsible for providing a slight 'W-like' shape in the middle of the data. The above data was taken at a completely different time than the data of figure 37. The interesting thing to note is that the approximate shape of the curve is very similar to that of figure 37, which was taken at a different time during construction. This further enhances the fact that buckling of the web is a localized phenomenon and the quality of data obtained with FBG sensors is accurate.

Next, we show and discuss data from other sensors in the array, including horizontally oriented sensors, diagonally oriented sensors and temperature sensors. An interesting question worth considering is that what influence does the buckling of the web have on the flange and how far does its influence extend in to the flange. What is the influence of the buckling on longitudinally oriented sensors on the lower web ?

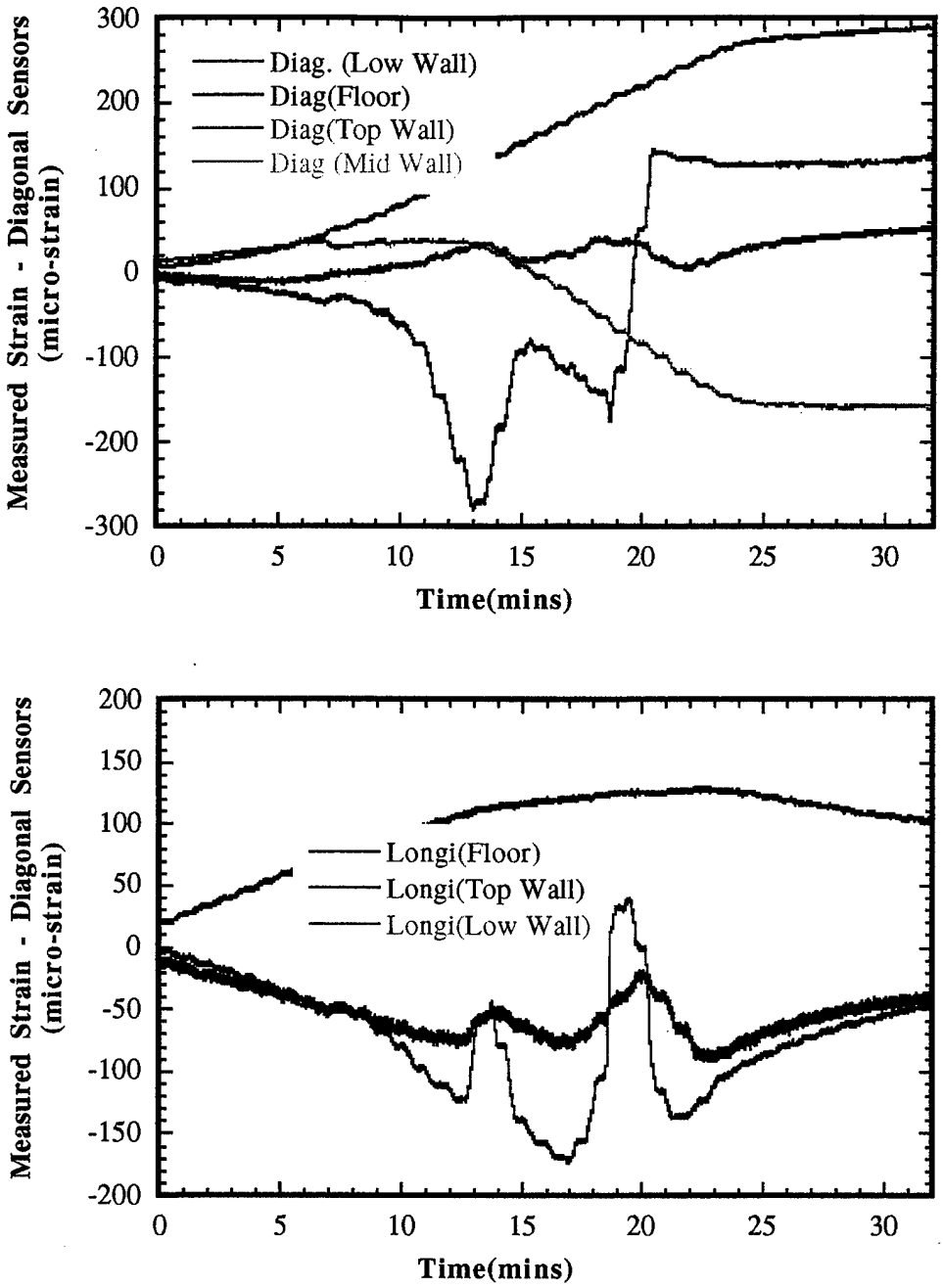

Figure 42. Measured strain responses from (top) diagonally oriented and longitudinally oriented (bottom) sensors during the push phase of October 1998.

The data from the longitudinally and diagonally oriented sensors on the box-girder show that the influence of the vertical loading, especially buckling of the web, is limited to the sensors which are in the immediate vicinity of the lower web. Not surprisingly, the diagonally oriented (red curve of figure 42-top) and horizontally oriented (green curve of figure 42 – bottom) sensors on the lower web show certain amount of strain which resembles the strain response of the vertically oriented sensor attached to the lower web (figure 37). This indicates that the strain in that region is dominated by the local buckling from vertical loading. In contrast, diagonally and horizontally oriented sensors located near the top of the web show little effect from buckling taking place near the bottom of the web. This shows that strain near the top is derived from more global effects occurring due to the push. Finally, the flange (i.e.floor) sensors which are close to the bottom web part show a combination of effects from localized buckling as well as global strain effects as can be seen from the curves shown in figure 42. The red curve shown in figure 42 (bottom), clearly shows the effects of buckling influencing the flange sensor response but in addition it also shows the effects of global strain in the box-girder. This is made clear by the fact that the longitudinally oriented sensor shows the 'W-like' curve from buckling taking place in near-by web but also has an overall all curvature to it, which is indicative of global strain changes occurring due to the box-girder being pushed.

For completeness, we show the response of temperature sensors during the push process. Figure 43 shows the response of the two temperature sensors, one attached near the top and the other attached near the bottom of the web. Significant temperature changes were not observed during the course of the push.

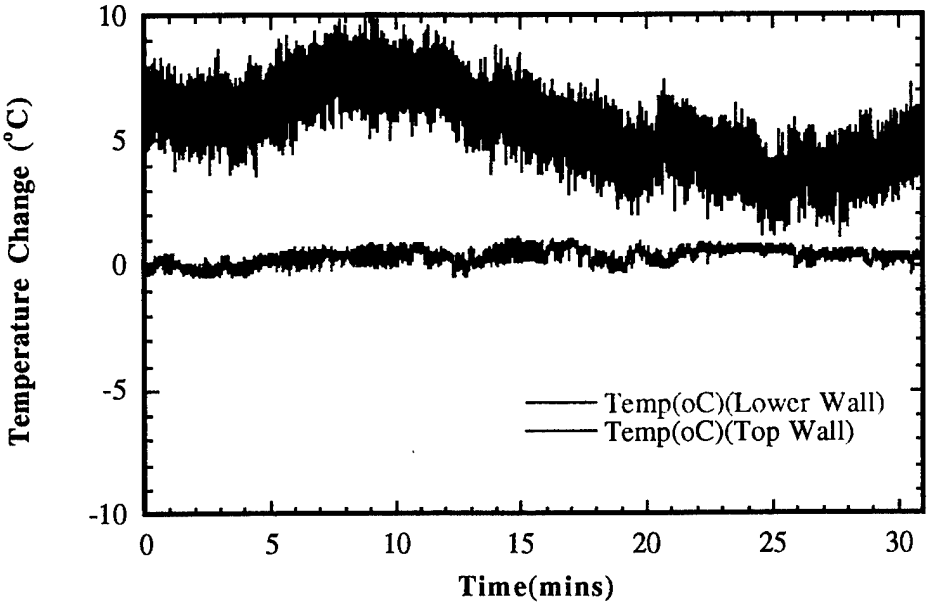

Figure 43. Temperature changes in the structure recorded over the period of the push. Absolute temperature at the time was approximately 4.5 °C..

Data of figure 43 shows measurements from two temperature sensors on the web. The temperature sensor mounted on the top wall appears to be quite noisy, on the order of a 3oC, which is quite large. Such noisy data from the gratings is indicative of the fact that the grating is not reflecting sufficient light back into the reading unit. This could be due to optical losses in the fiber line or can be a consequence of the optical source (1.3 micron ELED) shifting its spectrum sufficiently, due to thermal changes, that not enough light exists in the bandwidth of source spectrum coinciding with the Bragg grating. In other words, interpretation of data from the top wall sensor will not be made. However, the temperature sensor located near the bottom of the web does show low noise data. It is clear from the lower wall sensor that there is very little temperature change (< 0.5 °C) over the course of the measurement time.

In this section we have summarized the data from the push phase of October 1998. The data provided very useful information regarding the localized buckling due to vertical reactions from the pier as the box-girder passes over it. The buckling is indeed a localized phenomena since its influence does not reach the top of the web and also does not reach very far in to the flange region also. The buckling produces very large strain responses, however, all deformation appears to be within the elastic limit of the box-girder structure. Influences of global strain changes were also observed.

12. Lessons Learned and Future Recommendations:

As is the case with any successful field test performed with new technology, there are always issues, which surface during the course of the field test which have the potential to further improve the technology. We will briefly discuss some of those issues, which could help in improving array fabrication, speed up array installation and provide for improved results.

• During the February test of 1998, the FBG arrays were integrated at NRL prior to travelling to Switzerland. By array integration it is meant that a single line array consisting of Bragg gratings, with appropriate spatial and spectral separation were spliced together along with telemetry cables for strength and durability. The portions of the array containing the Bragg gratings were placed inside a hollow plastic tube for protection with the understanding that the tube will be slid off the Bragg grating part and the gratings will be bonded to at the appropriate locations on the bridge. While this array integration approach is a sound one from the point of view of array transportation, it suffered from two problems. The transition between the regions containing the Bragg gratings and the telemetry cable has such a huge difference in its stiffness that the fiber at the transition point could easily break during array handling on-site. The second problem was the use of the plastic tube for protecting the array. In cold climate, the plastic tube tends to shrink and stiffen, making it difficult to slide it off the array. This further endangers the Bragg gratings.Most of the times, the plastic jacket had to be ripped open with a specialty knife which could have broken the gratings as well. In many cases the array had to be spliced together on-site (more on this later), which should be avioded if at all possible. In future, it is recommended that the Bragg gratings and the telemetry cable not have such large stiffness difference, which could lead to fiber breakage during unspooling of the array on-site. If possible, the fiber line between gratings should be from regularly jacketed fiber (e.g. acrylate or nylon) so it is easy to spool or un-spool the array on-site. Follow this up

by using connectors at the end of the Bragg grating array from where heavy duty optical cables (e.g. plastic jacked cables with kevlar strands) can bring the signals to the reading unit. Avoid using the plastic tubing to protect the Bragg grating part. In fact, if regular jacketed fiber is used to connect between gratings then, there should be no need for any 'extra' protection of the part containing the gratings since it is already protected with acrylate coating.

• Splicing fiber in very cold climate can be problematic. In February 1998, which coincided with record cold temperatures in Switzerland for the year, the bridge surface and the atmosphere were so cold that small parts (e.g. rubber pads) in the cleaver stiffened sufficiently to not allow for a satisfactory cleave of the fiber. The cleaver had to be warmed with heating lamps for making cleaves which then allowed for satisfactory splicing to take place. In opposite conditions, like hot, dusty or windy environment it is also equally difficult to splice fibers. In general, the conditions at a construction site are not conducive for splicing optical fiber, thus if possible, planning ahead and fabricating the array in favorable environment can save significant aggravation later.

• In this work, we have traditionally used optical sources and gratings which operate at optical wavelength near 1.3 μm. While fundamentally it makes no difference which wavelength one operates, it makes a difference from a practical perspective. Typically, optical sources available at 1.3 microns produce low optical power. Though some new sources which rectify this have come in to the market recently. Because optical sources at 1.3 microns do not produce sufficient optical power, it seriously tests the noise characteristics of the reading unit and also limits the length of the telemetry cable. As is evidenced by the results of one of the temperature gauges of figure 43, low light levels from source in the bandwidth of interest generally means low light levels reflected back from the gratings. This increases the noise level from that specific grating []. It is recommended that in order to avoid such issues, until more powerful and reliable optical sources are available at 1.3 microns, all field tests should be carried out in the wavelength range of 1.5 microns instead of 1.3 microns. Optical sources at 1.5 microns are about one hundred times more powerful, more reliable and the issue of insufficient power in the array would be eliminated.

• 'Synchronize your watches' – if data are concurrently being taken with FBG sensors and other types of sensors and comparisons are expected to be made between the two at some later time, then time stamping both data sets is essential. This makes it significantly simpler, later to make fair comparison between the two data sets.

• In the February 1998 test, a number of gratings were used for temperature compensation of the strain data. As shown later, this turned out to be a waste of thermal gratings on a large metallic structure whose temperature does not change very quickly. In other words, use of temperature gratings is certainly required, however the density and positioning of thermal sensors should be done based on the size of the structure and by determining the potential for large temperature fluctuations in a given geographical area of the field test.

• The observations made in this part of the report have, we believe general validity during field testing of distributed Bragg grating sensor arrays.

• Finally, about man power. Unless help from local group can be relied upon field tests should be carried out with at least three personnel. The February 1998 test was carried out by two people which became physically quite challenging.

13. Conclusions:

Arrays of Bragg grating were used to measure the distributed strain response of an in-construction box-girder bridge. Measurements took place during two separate construction phases. Both phases involved pushing the box-girder forward over one of the piers such that it reaches the pier closest to the last one. This interesting and novel construction approach holds many advantages and is likely to see wide spread use in the near future. Obtaining strains in the structure during the push phase is therefore of paramount importance. Strain histories inside given locations of the box-girder were measured during these phases. Where possible, strain measurements as recorded by the Bragg grating system are compared to data from conventional gauges. Also where possible, an effort has been made to model the response of the structure for comparison with experimental data. This test has proved to be quite successful on many levels and we summarize them.

- The test of Bragg gratings and its associated instrumentation system (e.g. the Fabry-Perot reading unit) performed extremely well under fairly adverse conditions which included very cold temperatures, occasionally very windy conditions and rain.
- The strain histories at various locations inside the box-girder were recorded during various important phases of construction.
- Localized buckling of the box-girder was measured. No indications of the structure exceeding its elastic limit were measured, however if the structure had approached exceeding its elastic limit, the strain sensing system would have been well poised to warn the construction crew.
- The data from the Bragg grating strain sensing system agreed very well with that from conventional gauges with a few minor exceptions. It is unclear such minor descrepancies are due to errors in the reading unit of conventional system or is it due to two sensors not being perfectly co-located.
- The gratings which were attched to the structure during February 1998 were found be intact in October 1998 and in full operating ondition.

Arrays of fiber Bragg grating sensors are ideally suited for making distributed strain measurements on large scale structures due to their simplicity of installation, their small size, their built-in telemetry, high strain sensitivity as was evidenced by the fiedl test described in this report. All the advantages of a fiber sensing system were demonstrated in this field test. Two important obstacle need to be climbed still, one involves deligent notification to the community that field tests of Bragg grating strain sensing system indeed shows it to be superior to existing techniques in many ways and secondly to reduce the per channel cost of the system such that it becomes even more attractive to potential customers.

14. Acknowledgements:

Field tests in foreign lands are difficult by themselves but could become next to impossible without the help of some generous people on both sides. We acknowledge generous financial support of the federal highway administration (FHWA) , Mclean, Virginia. We are particularly indebted to Dr. Richard Livingston of FHWA for sponsoring and encouraging the project. We are also grateful to Dr. E. J. Frieble at NRL

for allowing us the free use of his Bragg grating fabrication facility. We also thank M. Putnam, C. Askins, C.C. Chang, M. LeBlanc and L. Malsawma at NRL for their technical support. We are particularly grateful to Mr. Nicolas Jean-Louis (construction site foreman) and his entire crew of Zwahlen and Mayr, Switzerland for allowing us free access to the box-girder and being very cooperative and understanding during the testing period even though they had much more important things to accomplish. We thank Dr. Daniele Inaudi of Smartec and Ecole Polytechnique De Federal Lausanne (EPFL) for initiating the project. We are also very grateful to Sam Vupilliot and Branko Glisic of EPFL who were always ready to help and provided us with invaluable assistance before, during and after the field test. We thank Mr. Miguel Gomez Navarro of ICOM-EPFL for providing us with conventional strain gauge data and taking the time to discuss structural issues associated with the project. We finally thank our families for their understanding and generosity but mostly for putting up with our crazy travel schedule.

15. References:

1. See for example, Proceedings of the 13th Optical Fiber Sensors Conference, B.Y. Kim and K. Hotate, editors, April 1999, Kyongju, Korea, SPIE Volume -----.
2. S.T. Vohra, C.C. Chang, B.A. Danver, B. Althouse, M.A. Davis and R. Idriss, in Fiber Optic Sensors for Construction Materials and Bridges, F. Ansari Editor, Technomic Publishing Co, p. 148 (1998).
3. R. A. Livingston, in Fiber Optic Sensors for Construction Materials and Bridges, F. Ansari Editor, Technomic Publishing Co, p. 3 (1998).
4. G.R. Meltz, W.W. Morey and W.H. Glen, Optics Letters 14, p. 823 (1989).
5. A.D. Kersey, M.A. Davis, H.J. Patrick, M. LeBlanc, K.P. Koo, C.G. Askins, M.A. Putnam and E.J. Frieble, J. Lightwave Technology, Vol. 15, p. 1442 (1997).